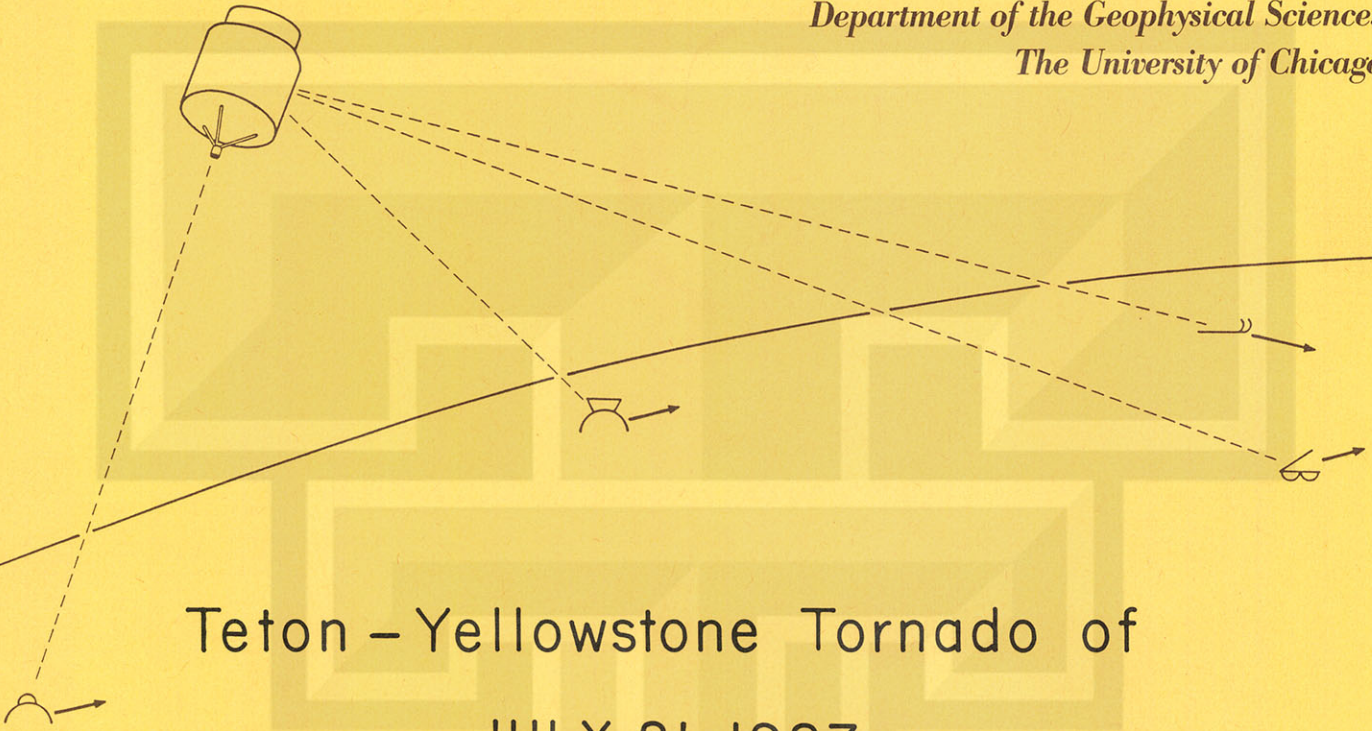


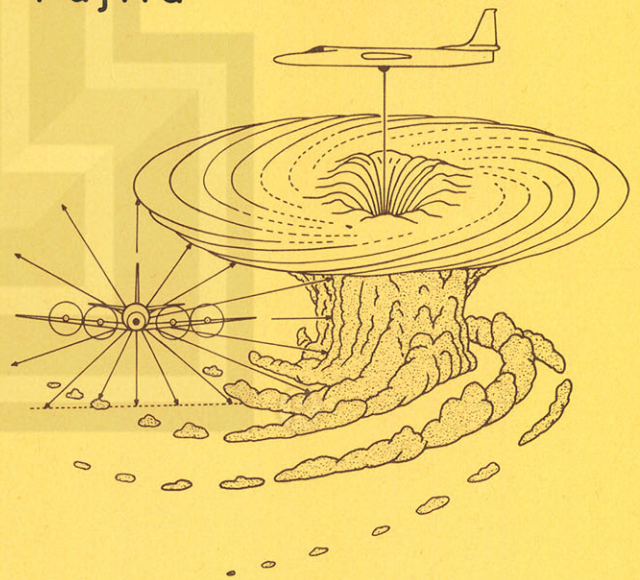
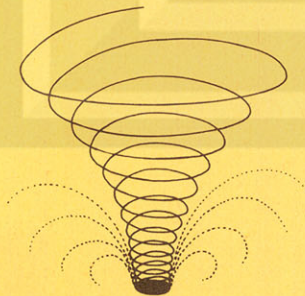
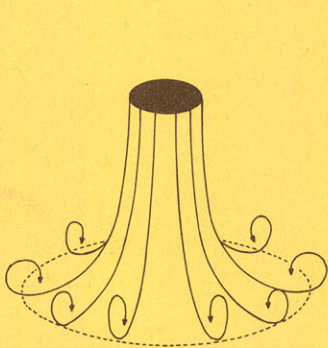
# WIND RESEARCH LABORATORY

Department of the Geophysical Sciences  
The University of Chicago



## Teton - Yellowstone Tornado of JULY 21, 1987

T. Theodore Fujita



## TETON-YELLOWSTONE TORNADO OF 21 JULY 1987

T. Theodore Fujita

The University of Chicago  
Chicago, IL 60637

### A B S T R A C T

The Teton-Yellowstone Tornado, rated F4, crossed the Continental Divide at 3070m, leaving behind a damage swath 39.2km long and 2.5km wide. A detailed damage analysis by using stereo-pair and color photos revealed the existence of 4 tornadic swirls and 72 microburst outflows inside the damage area. The tornado was spawned by a mesocyclone which formed at the intersection of a mesohigh boundary and a warm front. The parent cloud of the tornado, tracked by both GOES East and West, moved at 25 m/s and the number of cold-temperature pixels below  $-60^{\circ}\text{C}$  reached a peak during the tornado. While hourly analysis of surface maps were completed by using altimeter settings, upper-air cross sections up to 70mb were made, finding a mesoscale warm core of weak winds in the lowermost stratosphere above the severe thunderstorm clouds.

---

Corresponding author address: Prof. T. Theodore Fujita, Dept. of the Geophysical Sciences, The University of Chicago, Chicago, IL 60637.



## 1. Introduction

Although a number of tornadoes have been reported from the Rockies at high elevations, most damage paths are rather short and narrow in comparison with their Midwestern counterparts. An early report of a massive blowdown on 21 July 1987 in the Teton Wilderness indicated that one million trees in a 61 km<sup>2</sup> (15000 acres) area were uprooted. In order to document the rare damage for identifying the nature of the storm, the author arranged the following three survey missions:

30 JUL - 2 AUG 1987 An initial survey by James W. Partacz on board a Cessna aircraft, obtaining 430 color pictures.

19 AUG 1987 Contracted American Reprographics, Inc., to take 28 vertical, stereo-pair pictures on 23 X 23cm (9 X 9in) negatives. These pictures cover the entire area of the damage across the Continental Divide.

27 - 31 AUG 1987 After an inspection of these stereo-pictures, a detailed aerial photography from a low-flying Cessna was made by Brian E. Smith (940 photos) and the southernmost area was visited on foot by Bradley S. Churchill (90 photos).

These photographs literally show every single tree in the vast damage area extending from the Teton Wilderness to Yellowstone National Park. Examination of the aerial photos revealed that the damage was caused by a number of tornadic swirls and microburst outflows embedded inside an intense mesocyclone. It was decided that this complex storm should be called the Teton-Yellowstone Tornado, instead of a massive blowdown, with the F4 Fujita tornado scale.

Tornadoes in Wyoming are infrequent. Flora (1954) describes that only 61 tornadoes were reported in the 37.5 years ending with June 1953. This frequency is less than two tornadoes per year. The distribution of tornadoes between 1930 and 1978 in Fig. 1 reveals that most Wyoming tornadoes occurred on the east side of the Continental Divide, with lesser frequencies toward the Divide. From this statistical point of view, the 21 July tornado occurred at a most unlikely place, where a tornado of this intensity would not be expected to occur.

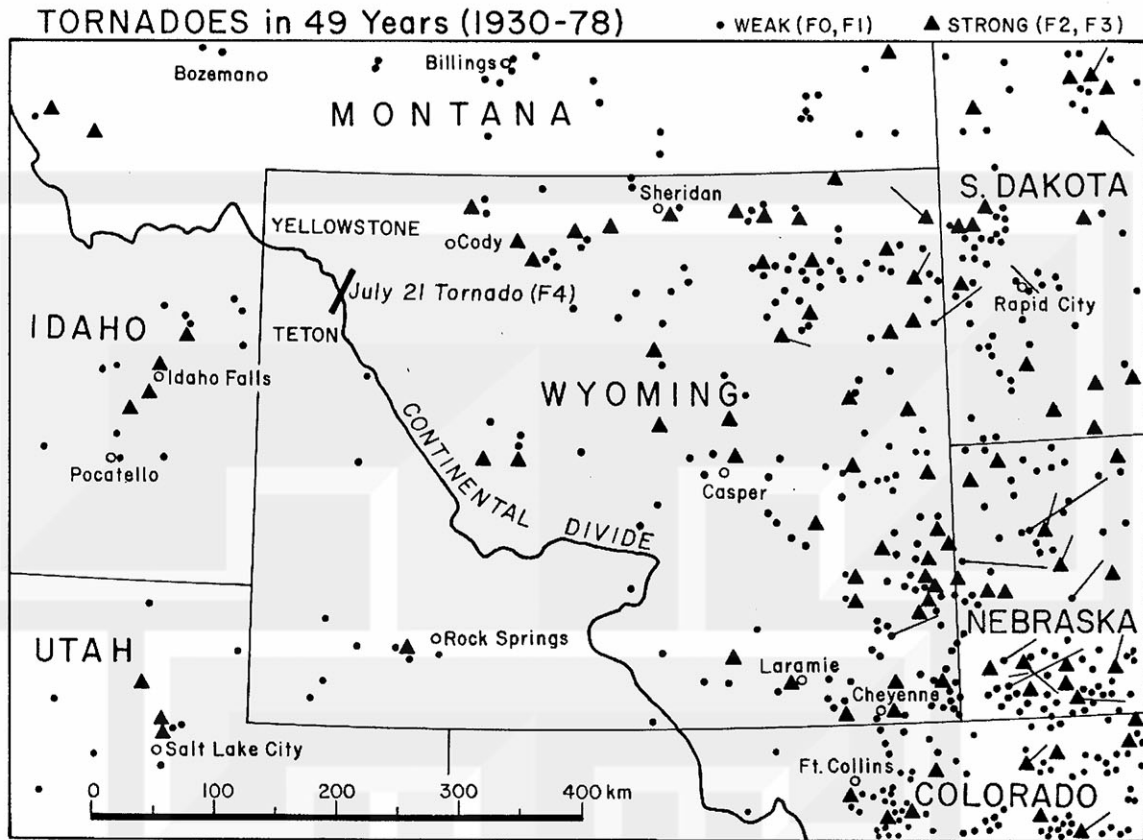


Fig. 1. Distribution of 191 tornadoes confirmed in Wyoming during the 49-year period, 1930-78. Average numbers are 3.9 per year. From U.S. Tornado Map by Fujita for National Weather Service Offices.

Like other meteorological phenomena such as drought, extreme heat or cold, etc., the distribution of tornadoes appears to be changing significantly. On 31 July 1987, ten days after this tornado, Edmonton, Canada was hit by an F4 tornado that killed 26 persons and injured over 300 others. On the other hand, not a single tornado was reported from the state of Oklahoma in April 1987 and again in April 1988.

As shown in Fig. 2, a large number of tornadoes in 1987 occurred in a horseshoe-shaped area, connecting the states: Florida - Mississippi - Texas (Panhandle) - Colorado - Minnesota - Michigan - New Jersey. No tornado was reported from Tennessee, located near the center of the horseshoe, whereas 11 tornadoes occurred in Wyoming in 1987.



Table 1. F-scale distribution of tornado frequencies in the U.S. during six years ending in December 1987, the year of the Teton-Yellowstone Tornado. From Fujita (1987) and Tornado maps (1986-87).

| Year | F0  | F1  | F2  | F3 | F4 | F5 | Total | F3-F5 |
|------|-----|-----|-----|----|----|----|-------|-------|
| 1982 | 375 | 433 | 172 | 58 | 6  | 1  | 1045  | 65    |
| 1983 | 355 | 370 | 146 | 57 | 4  | -  | 932   | 61    |
| 1984 | 369 | 353 | 130 | 41 | 14 | 1  | 908   | 56    |
| 1985 | 303 | 259 | 82  | 30 | 8  | 1  | 683   | 39    |
| 1986 | 352 | 270 | 114 | 22 | 3  | -  | 761   | 25    |
| 1987 | 337 | 245 | 60  | 12 | 3  | -  | 657   | 15    |

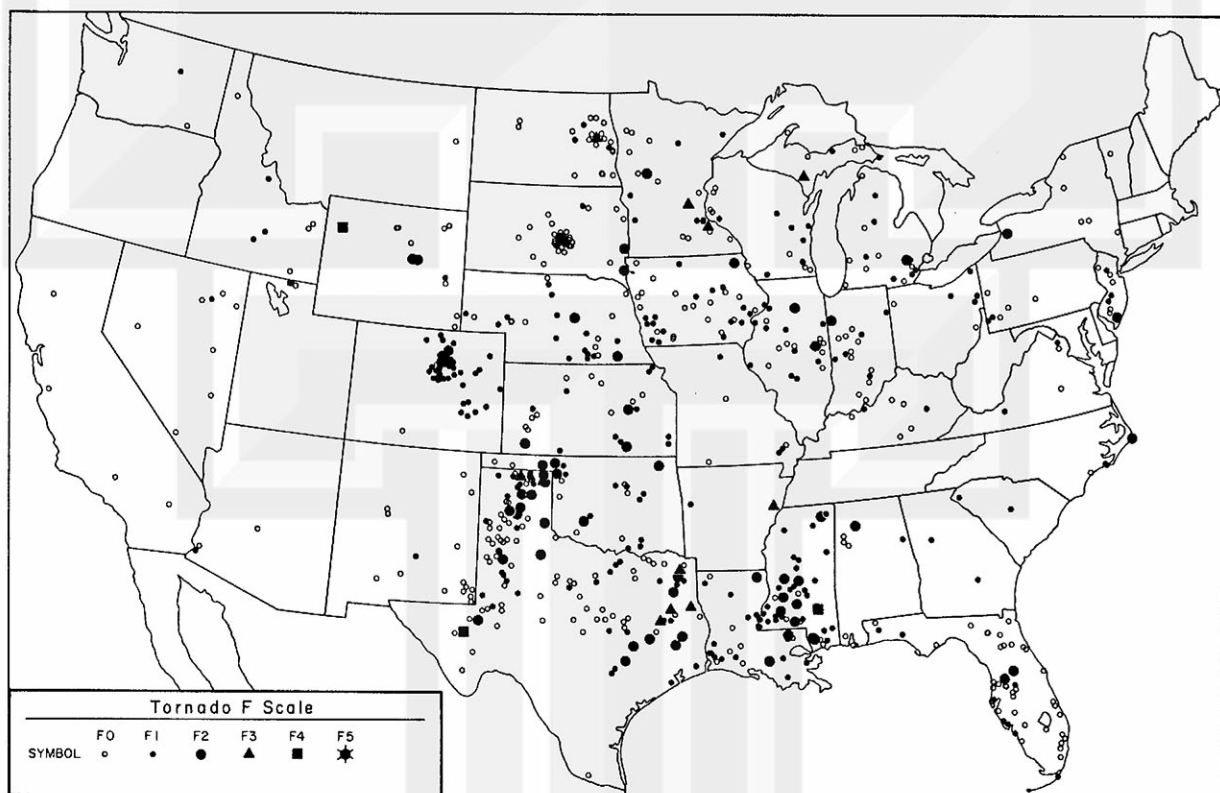


Fig. 2. A horseshoe-shaped distribution of tornadoes during 1987. Only 657 tornadoes were reported from the contiguous United States. For unknown reasons, activities from Kansas/Oklahoma to Tennessee were minimal this year.

It should be noted also that annual tornado frequencies, F3 or stronger in particular, in the contiguous United States kept declining during the 6-year period since 1982 (see Table 1). Although the reason for this declining frequency and change in activity areas has not yet been known, new statistical evidence suggests that tornado activities in the future could deviate significantly from the known statistical averages. In other words, a devastating tornado could occur at any unexpected area in the United States and southern Canada.

## 2. Mapping of the damage

In addition to the standard United States Geological Survey (USGS) 1:250,000 maps, three types of topographic maps were used in mapping the direction of fallen trees. These maps are:

### 1:24,000 USGS 7.5 MINUTE MAPS (south of 44°N)

Topography from 1964 aerial photographs, contour interval 40ft, forest areas in green.

### 1:62,500 USGS 15 MINUTE MAPS (north of 44°N)

Topography from 1954 aerial photographs, contour interval 80ft, forest areas in green.

### 1:126,720 FOREST SERVICE MAP (Bridger-Teton National Forest)

Compiled in 1984, contour interval 50m, no forest area indicated.

Two major problems encountered in using these maps are the difference in both scales and in contour intervals. The overall damage in Fig. 3 was mapped directly on the Forest Service map, while four local maps in Figs. 4 - 7 were made by enlarging and matching photographically the 15 MIN and 7.5 MIN maps into a unique scale. They were then re-mapped with a contour interval of 20 meters.

#### a. From touchdown to liftoff

The first indication of F1 damage was spotted in a valley 3 km to the northeast of Randolph Mountain. Thereafter, the damage path widened and became organized gradually toward the 2700m Gravel Ridge. There was a very large area of devastation to the northeast of the Ridge. The devastation continued toward Enos Lake, a beautiful emerald-colored lake at 2382m MSL. After passing directly over the lake, the storm descended into Pacific Creek Valley at 2380m MSL.

Damage on the cliff was visible between the valley floor and a 2900m plateau just to the north of the valley. The storm was on the plateau for several kilometers until it crossed the Continental Divide. The highest elevation of tree damage was confirmed at 3070m (10070ft) MSL on the Continental Divide.



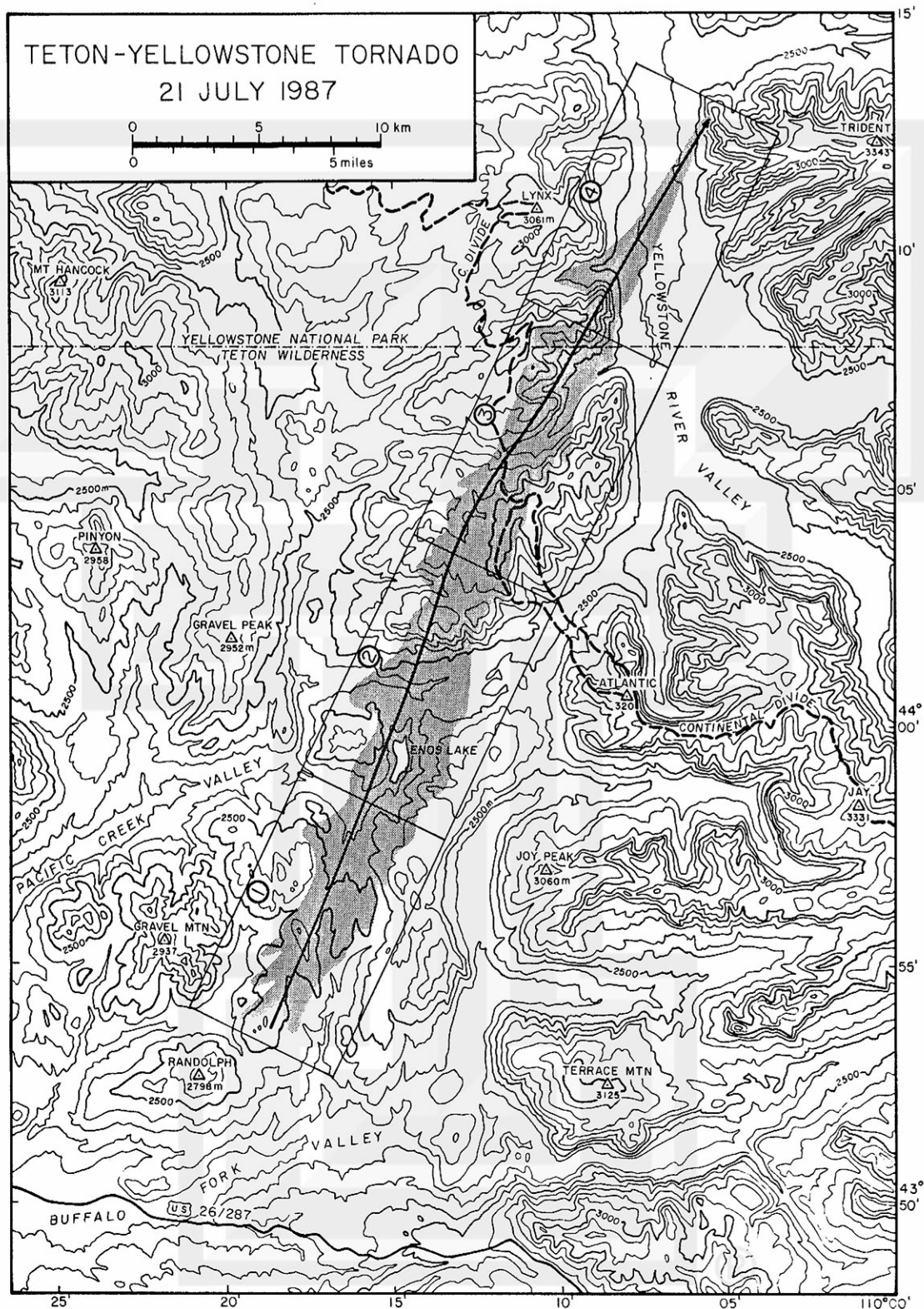


Fig. 3. An overall damage area of the Teton-Yellowstone Tornado which crossed the Continental Divide at 3070m (10070'). Detailed damage patterns inside the 39km-long and 2.5km-wide path are presented in four local maps 1, 2, 3, and 4.

Severe tree damage was seen inside three cirques, bowl-shaped depressions carved by glacier. After descending from these cirques, the storm crossed the headwaters of Falcon Creek and the path went up and down a number of cliffs until descending to the floor of the Yellowstone River Valley. Storm winds weakened gradually while passing over the flat valley floor at 2400m MSL. On the other side of the valley, damage became spotty until wind effects disappeared on the slope at 2520m MSL.

The Teton-Yellowstone Tornado left behind a 39.2km (24.4mi)-long path with an average width of 2.5km (1.6mi), devastating the protected forest of the Teton-Yellowstone Wilderness. The highest F-scale damage confirmed inside the tornado area was F4, an intensity rarely experienced in the Rockies.

Small spotty areas affected by F4 winds were characterized by flattened Engelmann spruce trees, 30 to 40 cm in diameter, spattered by wind-blown topsoil and debarked.

#### b. Four local damage maps

The overall damage area in Fig. 3 was divided into four rectangular areas, Maps 1, 2, 3, and 4. Each area was enlarged and re-mapped with contour lines at 20 m interval and forest areas were added for determining the location and the fall direction of damaged trees.

Map 1 in Fig. 4 covers the damage area from touchdown to the Enos Lake area. The most interesting damage pattern seen in this map is the existence of 18 centers of diverging winds. These centers are located predominantly on top of small hills, but some are found in valleys. It is suspected that the diverging winds on the ground were induced by an incloud downdraft as it was intercepted by high-elevation terrain extending into the storm cloud.

From the genetic point of view, a system of diverging winds on the ground is a microburst proposed and studied by Fujita (1981). When observed individually, a microburst over a forest will induce a so-called blowdown, reported widely from forested areas in mountains. Over the Midwest however, the ground, located far below the convective cloud base, is an ineffective interceptor of downdrafts which are diffused and weakened after the long-distance descent through subcloud layers.



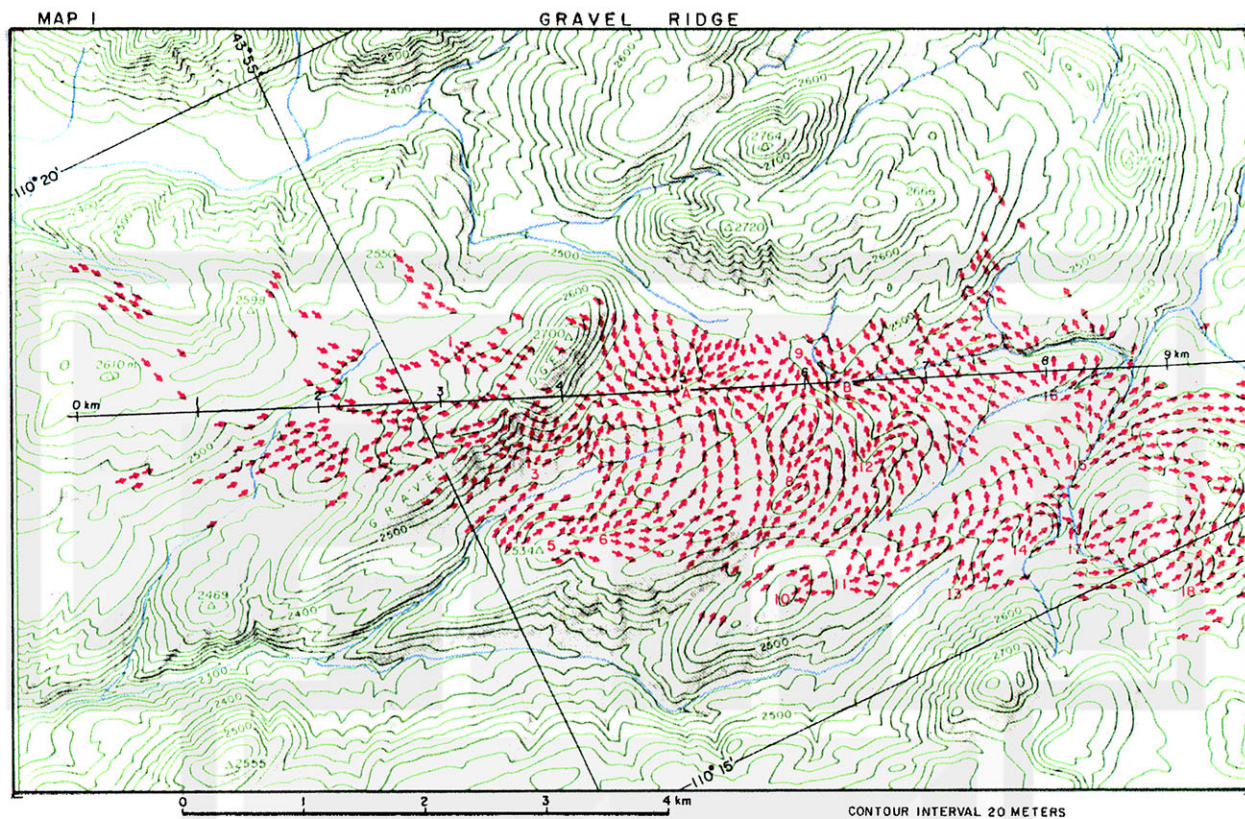


Fig. 4. Gravel Ridge Section covering 0.0 to 9.7 path kilometers. Tornadic Swirl A and B and 18 microbursts are in this map.

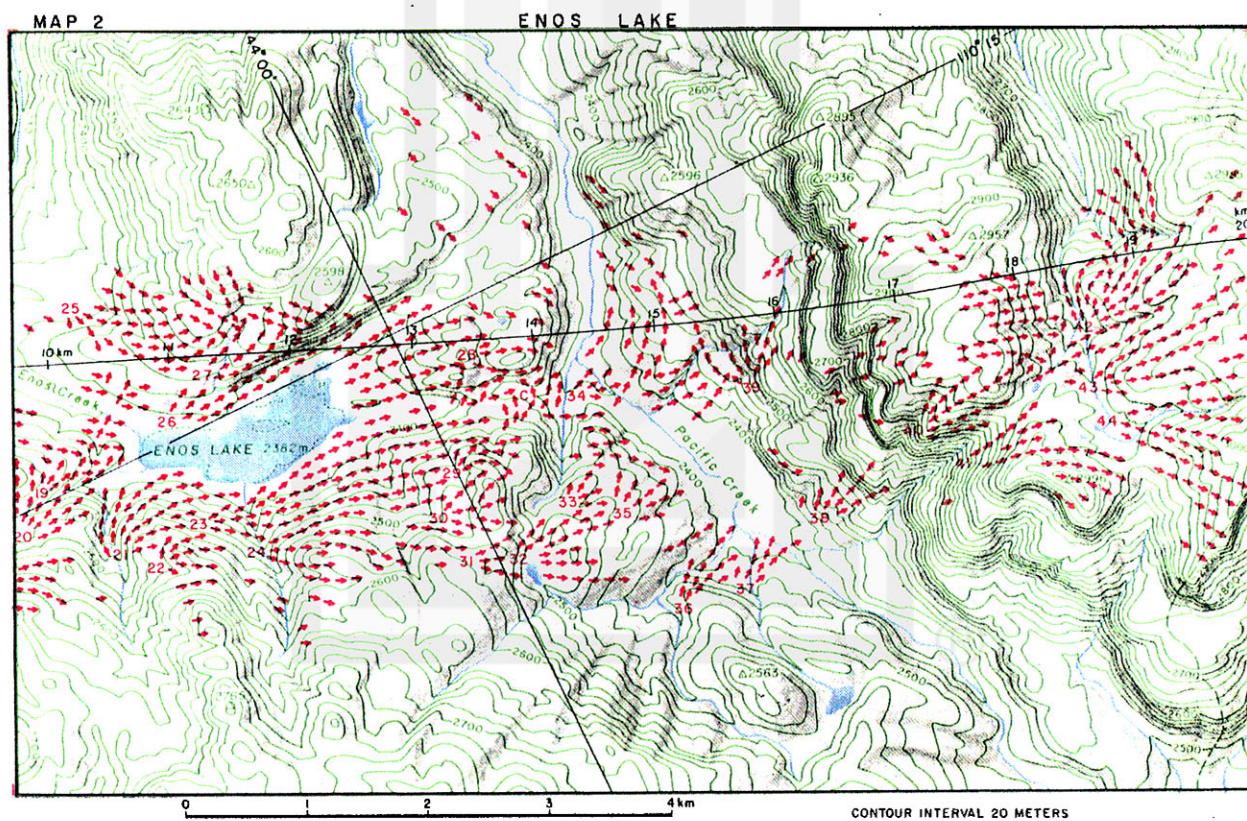
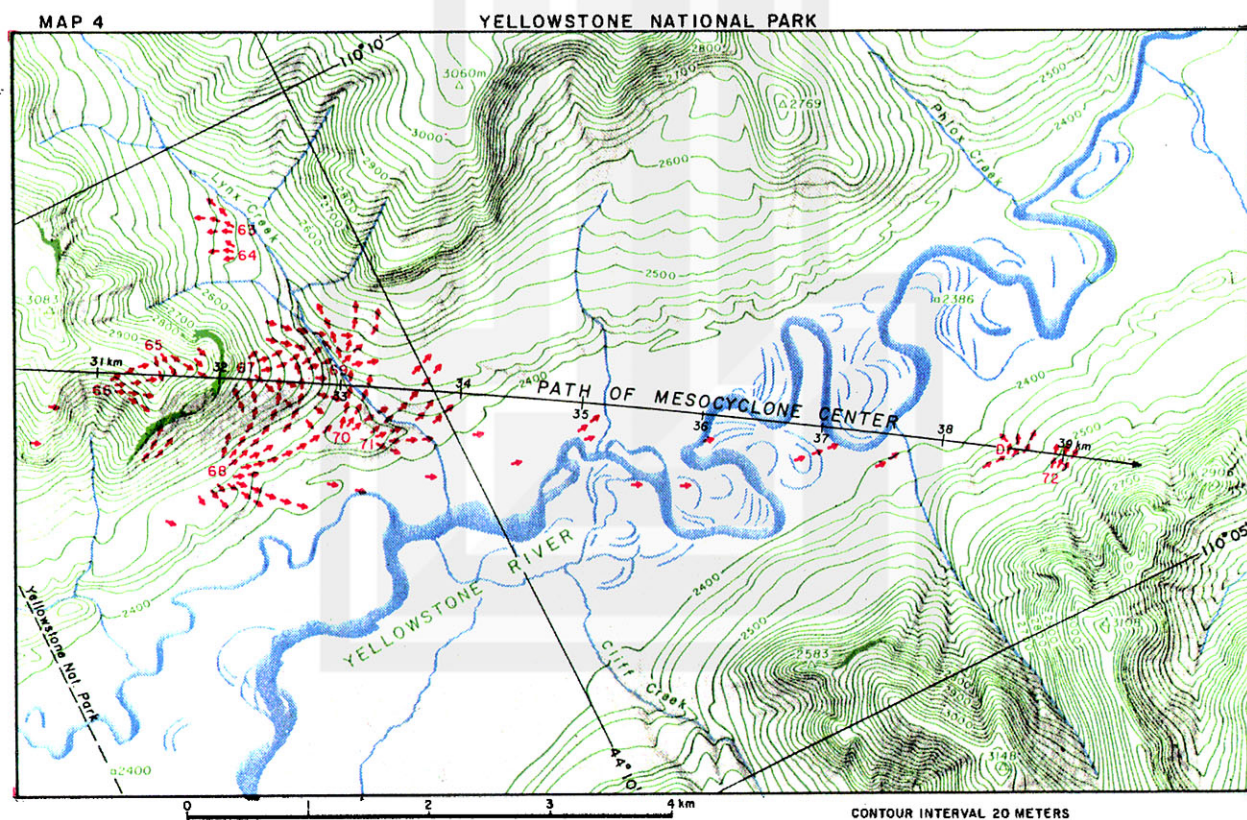
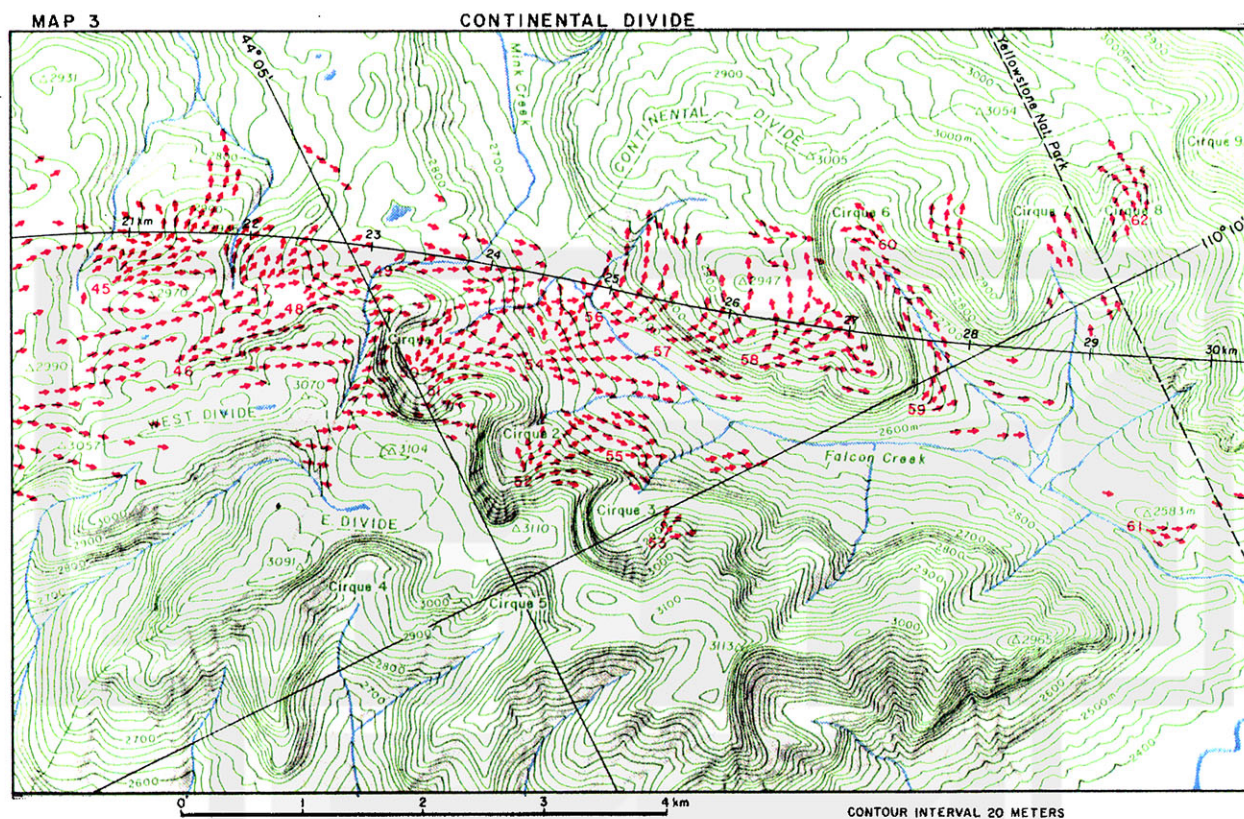


Fig. 5. Enos Lake Section covering 9.7 to 20.0 path kilometers. Tornadic Swirl C and 26 microbursts are in this map.







It will be shown later that the parent cloud of this windstorm traveled at the rate of 25 m/s, from left to right across the local map. When intercepted by the ground, incloud downdrafts will move from left to right on the map at a high translational speed, resulting in an airflow skidding toward the storm motion.

Apparently, the parent cloud was rotating as it moved across Map 1. The airflow, diverging out from each microburst, was spiraling in toward the rotation center of the parent cloud. In other words, the rotational winds made visible by the directions of fallen trees are those of a mesocyclone.

Where were the tornadoes? Over the Midwestern plain, microburst-induced tornadoes move with the parent storm leaving behind either intermittent or continuous damage swaths. Inside this map, however, only two tornadic swirls, A and B, are visible along the path of the mesocyclone center. It is unlikely that a slow-rotating tornado would leave behind a swirling pattern of fallen trees, because the translational speed of the parent storm was estimated to be 25 m/s (56mph). Furthermore, narrow swaths of tornadoes could be wiped out by high winds of subsequent microbursts.

Map 2 in Fig. 5 includes the damage area from near Enos Lake to the plateau top, north of Pacific Creek. Centers of Microbursts 19 through 44 are seen in this map. Damage vectors show that some microburst centers are located on the upwind side of the steep slope, and the diverging winds blew upslope violently over cliffs in rugged terrain.

The mesocyclone center entered the left edge of this map at 9.7 path kilometers (distance measured from the first damage) and departed the right edge at 20.0km, passing north of Enos Lake. At two locations, one in Pacific Creek Valley and the other on the plateau, the rotational characteristics of the mesocyclone are clearly visible. It should be noted that these curved outflows originated in Microbursts 34 and 42, suggesting strongly that a large number of microbursts around the mesocyclone center were the providers of the angular momentum required to maintain the mesocyclone circulation against large orographic friction in boundary layers.

Tornadic Swirl C was identified in a forest south of Pacific Creek. It was characterized by both swirling and random tree damage, implying that a large tornado had been at a stationary position over the forest for a while.

Map 3 in Fig. 6 extends between path kilometers 20.0 and 30.3 of the mesocyclone center. Swirling airflows were originated by Microbursts 45, 54, 56, 57, 58, 59, 60, and 62. These microbursts comprise 45 per cent of the 18 microbursts that descended in the area of this damage map.

Of interest is the descent of four microbursts inside Cirques 1, 2, and 3. Each of these microbursts descended near the eastern side of each cirque. The similarity in the location of these in-cirque microbursts, relative to the cirque, suggests a significant role of the geometry of the cirque in inducing these microbursts.

Map 4 in Fig. 7 includes path kilometers between 30.3 and 39.2, the end of the path. Ten microbursts, 63 through 72, are shown in this local map. The area of the most active microbursts is seen to the south of the Yellowstone River. Two microbursts, 65 and 66, descended near the top of a 2950m hill surrounded on three sides by sheer walls of rock. Microburst 67 landed at the foot of the sheer wall on the downwind side. Three more microbursts descended farther downwind toward the river.

Microburst activities on the river valley were insignificant, and no evidence of microburst was found on the valley floor, in spite of the fact that numerous trees were seen in the aerial photos. The final stage of the mesocyclone wind was evidenced on the north-side slope of the Yellowstone River Valley. Tornadic Swirl D was confirmed at 2450m MSL and Microburst 72, the last microburst, was found on the path of the mesocyclone center at 2500m MSL. The overall damage swath of the Teton-Yellowstone Tornado ended at the 39.2 path-kilometer point.

#### c. The F4 damage

Damage patterns left behind by the Teton-Yellowstone Tornado are categorized into (1) tornadic swirl, up to 200 m in diameter, (2) microburst outflow, 1 to 3 km in major axis, and a much larger (3) mesocyclone circulation, 2 to 5 km in radius of curvature. These three damage patterns are woven together by a succession of high winds into a huge carpet of fallen trees.

The vertical photograph in Fig. 8 covers 1.8km X 2.3km area to the north of the 2700m Gravel Ridge. Centers of five microbursts, Numbers 4, 6, 7,



Fig. 8. A portion of the vertical picture #7, one of the 28 stereo pictures taken by a photographic aircraft on 19 August 1987, 29 days after the storm. An estimated 130,000 trees were blown down in the area of this picture.

8, and 9 are identified in this picture, along with Tornadic Swirl A located on the path of the mesocyclone center, extending from left to right across the upper section of the photograph. This photo is a cut-out from a sequence of 28 vertical stereo photos taken on 19 August 1987.

A band of light brown color extends from left to right just below the path of the mesocyclone center. The band denotes the F4 damage (band of F4 winds) caused by the tornado as it traveled side-by-side with the mesocyclone center. The swirling pattern expected to be seen in this band is not identifiable due to damaging winds which occurred later. The band of F4 winds is characterized by uprooted large trees, spattered by wind-blown topsoil and debarked. This band is visible in an oblique aerial photo in Fig. 9 taken from a distance of 2 km. It extends from left to right across the center of the picture on a gentle hillside.

The damage weakened toward Enos Lake drained by Enos Creek as seen in Fig. 10. The photo, looking south-southeast, shows high mountains along the Continental Divide and the 3060m Joy Peak in the background. Light-colored forests on the other side of Enos Lake are those damaged by Microbursts 22, 23, 24, 29, 30, and 31. The mesocyclone center moved from left to right, on the slope of the foreground hills obscured in this oblique aerial photograph.

A close-up of Tornadic Swirl A is shown in Fig. 11. Although a distinct swirl is seen approximately 2 cm above two spots of bare ground, evidence of other swirls are also visible elsewhere in this picture. Fallen trees in the lower right were stripped of most leaves and branches and trunks were debarked. The author has not seen such a devastating tree damage in the vicinity of the structural F4 damage in cities such as Xenia, Ohio and Birmingham, Alabama which he had investigated. The only F4 damage in a forest comparable to this one was photographed from a Cessna by the author in the Appalachians after the F4 Murphy Tornado in North Carolina on 3 April 1974.

Typical blowdown damage by a microburst is seen in Fig. 12, photographed half-way between the centers of Microburst 8 and Tornadic Swirl A. The microburst center is located below the bottom of this photo and its outburst winds flattened tall trees, blocking the major Enos Lake Trail that extends





Fig. 9. A band of F4 damage visible as a band of light brown color, extending left to right on small, low hills. (Photo by James W. Partacz)



Fig. 10. A view of emerald-colored Enos Lake. Seen in the background are high peaks on the Continental Divide. (Photo by James W. Partacz)





Fig. 11. A close-up view of Tornadic Swirl A made visible by a swirling pattern of blown-down trees. (Photo by Brian E. Smith)

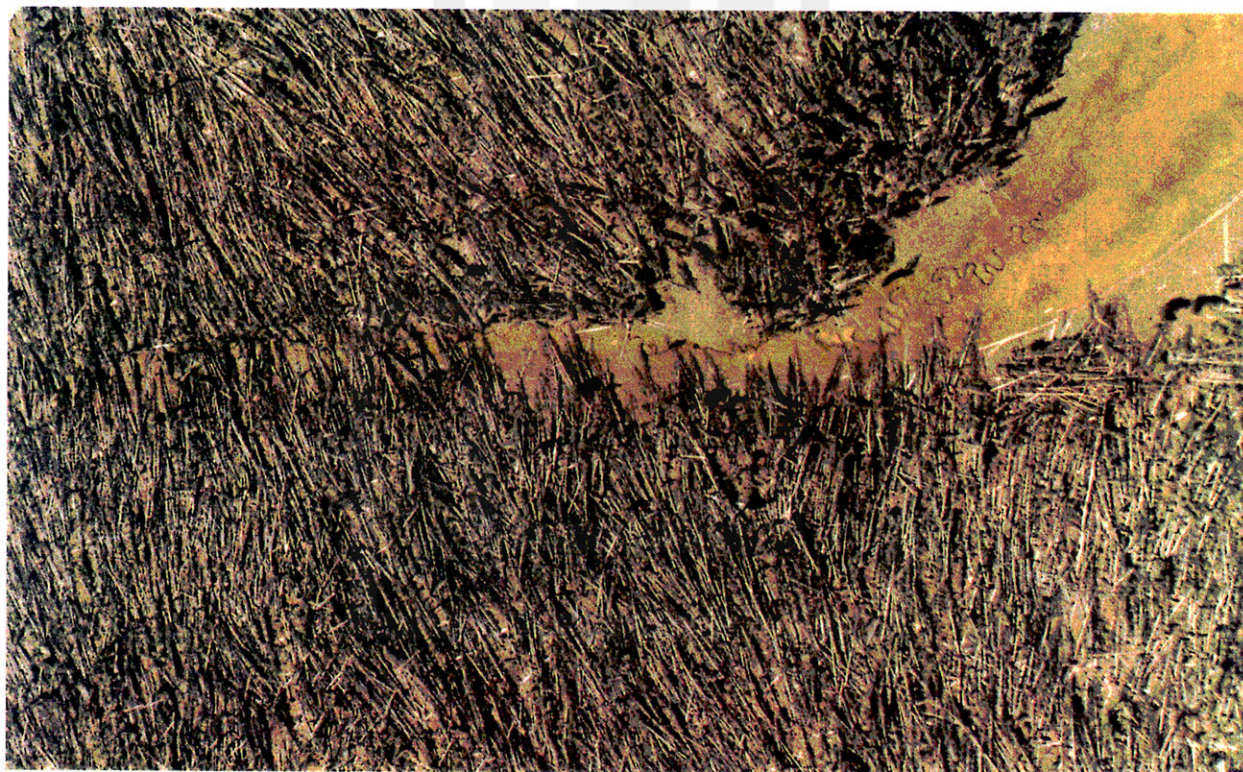


Fig. 12. A close-up view of blown-down trees inside Microburst 8. Fallen trees blocked Enos Lake Trail. (Photo by Brian E. Smith)



across the photo into a meadow. It is amazing to count 2700 trees uprooted in the area of this photo covering  $0.08 \text{ km}^2$ . The prorated number of trees blown down in the  $4 \text{ km}^2$  area in Fig. 8 is 130,000. A total of one million trees were blown down by the storm.

#### d. Microbursts in cirques

Three cirques near the Continental Divide are located on the east side of the path of the mesocyclone center (see Fig. 13). The center of Cirque 1 is located 0.9km away from the path, Cirque 2, 1.6km, and Cirque 3, 1.9km. A detailed analysis of damaging winds in and around these cirques revealed the existence of a microburst or a microburst family inside each cirque. Furthermore, positions of the microbursts relative to the cirque headwalls are almost identical.

Because the downflows inside the mesocyclone did not know where cirques were located beneath them, it is very unlikely that this microburst-cirque relationship was accidental. In an attempt to explain this relationship, it was hypothesized that the slanted downflow reaching the plateau of the pre-glacial surface slides down the surface of the headwall. The bowl-shaped surface will deflect the downflow into a focusing airflow which turns into a microburst upon reaching the ground inside the cirque (see Fig. 14). Table 2 was prepared to present geographic data applicable to these microbursts in three cirques. Note that the angle of descent of the focusing winds vary between  $13^\circ$  and  $25^\circ$ . Note also an increase in the F-scale microburst winds toward the path of the mesocyclone center.

The mechanism of microburst formation will work when a downflow descends toward the concave point of a headwall. Other downflows reaching unfavorable locations may not turn into microbursts unless the flowspeed exceeds a threshold value. In other words, the cirque acts as a booster of microburst winds.





Table 2. Microburst winds in three cirques focused by arc-shaped headwalls. Microbursts are seen at the focal points inside cirques.

|                              | Cirque 1 | Cirque 2 | Cirque 3 |
|------------------------------|----------|----------|----------|
| Height of headwall (m MSL)   | 3030     | 3100     | 3110     |
| Height at microburst (m MSL) | 2860     | 2880     | 2980     |
| Height of descent (m)        | 170      | 220      | 130      |
| Headwall to microburst (m)   | 410      | 470      | 580      |
| Angle of descent             | 23°      | 25°      | 13°      |
| Microburst damage            | F3       | F2       | F1       |

#### e. Angular momentum of mesocyclone over rugged terrain

Mesocyclones in the Midwest have been detected by radars as characteristic hook echoes for tornado warnings. For example, the effective warning of the Topeka, Kansas tornado was achieved by Garrett and Rockery (1962) based on the hook. Since Brown et al. (1971) succeeded in the Doppler detection of mesocyclone, Doppler-detected mesocyclone became the most important feature for use in tornado warnings. Burgess et al. (1976) detected mesocyclones with a 30min average lead time before tornadoes. In the Rockies however, mesocyclone detection even by advanced radars will be extremely difficult. First of all, both ground clutter and obstruction by mountains will result in blind spots and second, we still do not know the mechanism of mesocyclone formation over rugged terrain.

How can a mesocyclone maintain its circulation against large frictional forces in the boundary layer over rugged terrain? The top diagram in Fig. 15 presents the elevation of the damage area along the damage centerline. The middle diagram depicts isolines of F-scale winds estimated from degradation of the tree damage. Apparently, the mesocyclone intensified during the first 3 min while traveling from 0 to 4 path kilometers at 25 m/s. The peak intensity was maintained during the following 7 min, between 4 and 14 path kilometers. It then weakened significantly while passing over the 2900 to 3000m plateau. After leaving the plateau, strong microbursts were confirmed in the area of the three cirques. Thereafter, it weakened gradually, leaving behind a number of small F2 microbursts on and below the sheer cliff on the west side of the Yellowstone River Valley.

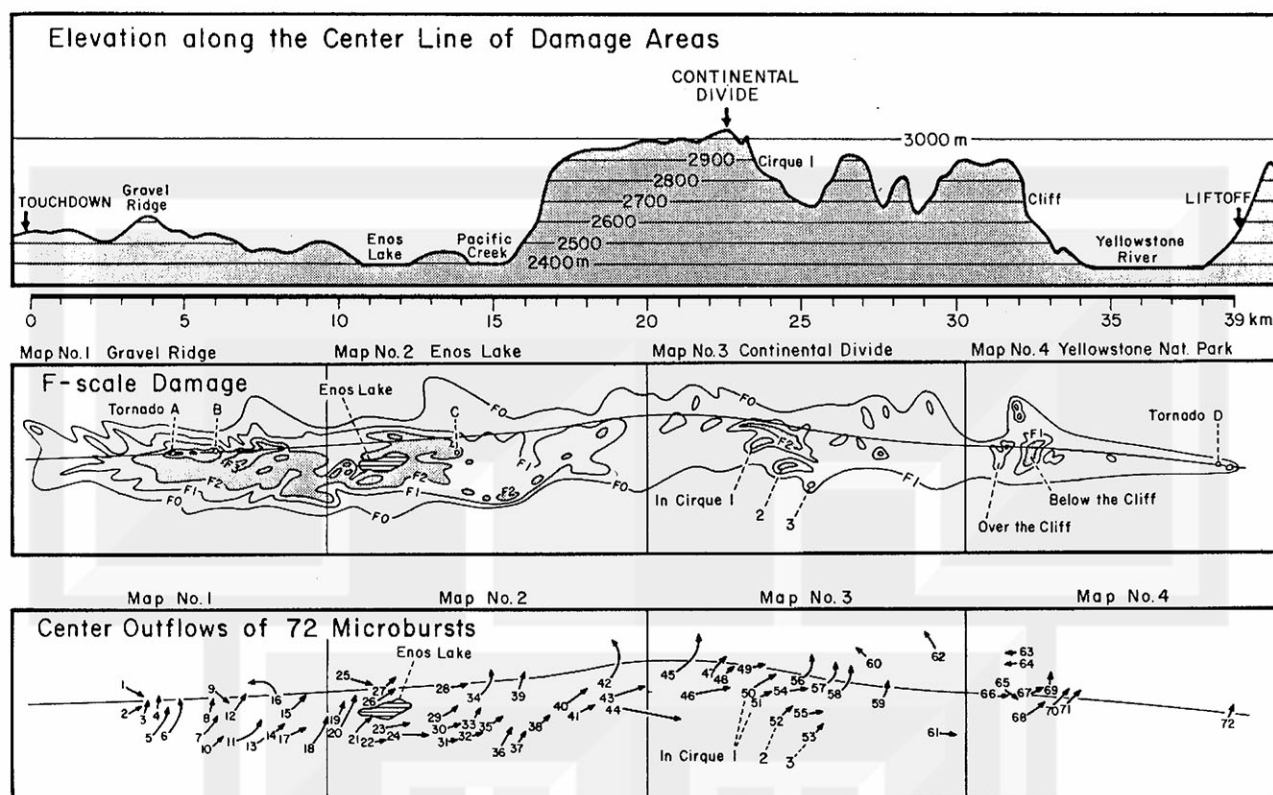


Fig. 15: Top: Elevation of the ground along the center line of the damage area. Middle: F-scale isotachs inside the damage area. Bottom: Center outflows of 72 microbursts, contributing to the impulsive addition of angular momentum.

The foregoing evidence confirms that the mesocyclone worked hard in maintaining its circulation. The strong circulation over the rolling hills during the first ten min weekend while traversing over the Continental Divide, indicating the importance of the balance in the supply and loss of angular momentum.

The bottom diagram of Fig. 15 presents the center outflows of all microbursts in relation to the path of the mesocyclone center. This diagram suggests convincingly that the angular momentum of the mesocyclone was supplied by microbursts as their outburst winds spiraled into the mesocyclone center. As expected, a strong microburst at a proper distance away from the mesocyclone center is most effective in achieving an impulsive addition of angular momentum for intensifying the mesocyclone.

In learning more about the impulsive addition of angular momentum, Fig. 16 was produced by re-locating all of the 72 microbursts inside the damage

area on coordinates relative to the cyclone center. The position of each microburst was determined by shifting the microburst center along its path until the center outflow coincides best with the hypothetical spirals encircling the mesocyclone center. This diagram reveals that microbursts in the right-front quadrant contributed most, followed by those in the right-rear, left-front, and left-rear quadrants of the mesocyclone.

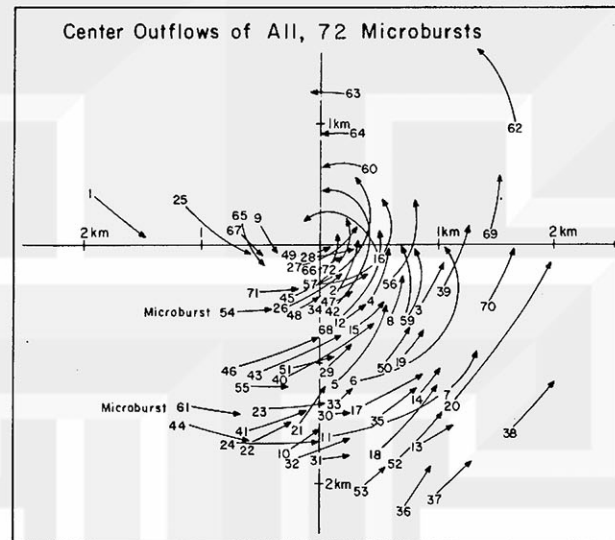


Fig. 16. Mesocyclone-relative positions of 72 microbursts and their center outflows.

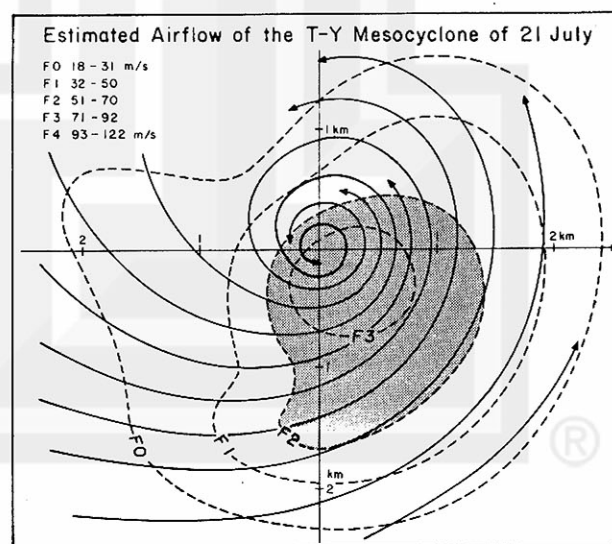


Fig. 17. Airflows and F-scale isotachs inside the mesocyclone in mature stage.

Keeping this in mind, we shall examine the bottom diagram of Fig. 15 once again. It is seen that most microbursts during the formative and mature stages occurred in the right-front quadrant where the supply of angular momentum by microbursts was most predominant. The location of microbursts as well as the orientation of center outflows during the traverse over the plateau was not favorable in supplying angular momentum. Based on Figs. 15 and 16, the airflow and F-scale isotachs inside the mesocyclone at its mature stage was reconstructed in Fig. 17.

It is likely that there is a feedback mechanism by which a strong mesocyclone induces more microbursts, while a weak one induces fewer microbursts. Through this re-cycling process, a strong mesocyclone is able to maintain its strength, even over rugged terrain. Needless to say however, the analysis of this mesocyclone generated more questions than answers.

### 3. Surface weather observations

The first isolated tree damage related to this storm cloud was confirmed near Teton Village 7km west-southwest of the Jackson Hole Airport (JAC). The direction of tree damage was  $280^\circ$ . On the other hand, JAC reported at 1310MST an 18 m/s wind with a 26 m/s (58mph) gust from  $280^\circ$  during a severe thunderstorm with hail. It is likely that the Teton Village winds occurred in advance of the JAC wind, but there was no evidence of a tornado.

#### a. Was the tornado accompanied by a funnel cloud?

Surface weather observations of this storm were made at the Jackson Hole Airport located 46km (29mi) southwest of the first damage. According to the observation log in Table 3, an overcast ceiling was at 2.4km AGL (4.4km MSL) and lasted from 1300 to 1550 MST. This MSL height is identical to that of the convective cloud base computed from the 00GMT (1700MST) sounding at Lander (LND), Wyoming. During the stormy weather at JAC between 1300 and 1345MST, a lower ceiling at 900m AGL (2900m MSL) was also observed. This height represents the storm-cloud base, commonly seen beneath a cumulonimbus cloud. It is suspected that the storm-cloud base around the mesocyclone center under investigation could have been much lower than the 2900m MSL observed at JAC.



Table 3. Surface weather observations at Jackson, Wyoming.  
 Period: 1045-1550 MST 21 July 1987. Ceiling in 100m, S-scattered,  
 B-broken, O-overcast, X-obscured, E-estimated, ff in m/s.

| MST  | GMT  | Clouds and ceiling | Weather  | Temp | ddff |
|------|------|--------------------|----------|------|------|
| 1045 | 1745 | E9-B 31-0          | R-       | 12°C | 0000 |
| 1146 | 1846 | 8-S 15-B 31-B      |          | 15   | 0000 |
| 1245 | 1945 | 12-B 24-B 37-0     |          | 16   | 0403 |
| 1300 | 2000 | 9-B 24-0           | TRW-     |      | 0305 |
| 1310 | 2010 | 0.3-X RAIN         | TRW HAIL |      | 2818 |
| 1320 | 2020 | E9-0               | TRW-     |      | 3008 |
| 1345 | 2045 | E9-B 24-0          | TRW      | 11   | 1606 |
| 1447 | 2147 | E12-B 24-0         | TRW      | 12   | 1605 |
| 1550 | 2250 | E21-B 24-0         | RW       | 11   | 1803 |

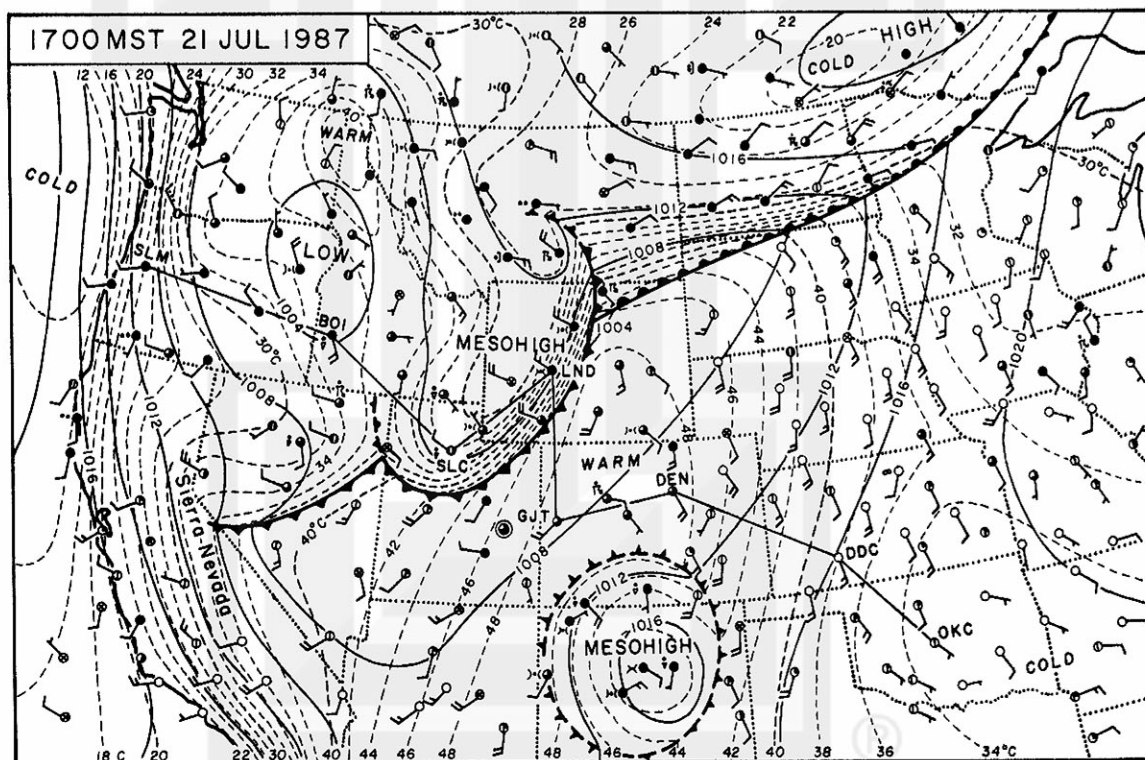


Fig. 18. A re-analysis of the NMC surface map at 1700MST (00Z) with isotherms of potential temperatures in °C. The Teton-Yellowstone Tornado ended approximately 3 hours before this map time.

It is quite possible that the mesocyclone cloud base was below the elevation of Enos Lake at 2382m MSL, and the entire damage occurred just above the cloud base. Consequently, no funnel cloud existed while destructive winds were on the ground. Witnesses to the storm, in a group of nine, on a camping trip near Enos Lake said they saw no funnel cloud and that the storm happened very quickly with a roar like a train in the distance. They noticed that golfball-sized hail pelted the ground. No other eyewitness has been found, so far, because one must walk or ride a horse for 5km from the nearest road to the damage area.

b. Mesohigh and cold front

Early in the morning of 21 July 1987 at 05MST (12Z), a cold front extended toward the southwest from the center of the 1001mb cyclone over Hudson Bay, Canada. A small low-pressure area was located in northwestern Wyoming at the tail end of the cold front. Seen also on the surface map are thermal lows over the desert regions of Arizona, Nevada, and Oregon. There was a strong moisture inflow along the east side of these thermal lows where 13°C dew-point temperatures were reported.

Thunderstorms began at Ely, Nevada at 0450MST (1150Z) and at Salt Lake City, Utah at 0429MST (1129Z), lasting two to three hours. The first sign of the mesoscale high pressure area (mesohigh) formed in southern Idaho and expanded into a 450km X 850km sized mesohigh at 17MST. The surface map at 17MST (00Z) in Fig. 18 shows the large mesohigh on a cold front extending from Montana to the Sierra Nevada. Another mesohigh is seen over New Mexico. This map is a re-analysis of the NMC surface map at 00Z and isobars were drawn at 4mb interval. Because the elevation of some stations in the Western Regions exceeds 2000m MSL, isotherms of potential temperature in °C were drawn instead of temperature isotherms. As expected, a 15°C cooling in potential temperature is seen inside the large mesohigh centered over western Wyoming. A line connecting OKC-DDC-DEN-GJT-LND-SLC-BOI-SLE was used later in producing vertical cross sections.



### c. Mesoanalysis with altimeter setting

Time plots of hourly and special observations depicted an early stage of a mesohigh in southern Idaho at 09MST. It expanded rapidly toward the northeast, passing the tornado area shortly before 14MST (see isochrones in Fig. 19).

In order to achieve a mesoanalysis over high terrain, we have to make use not only of the hourly but also special observations during weather events. Unfortunately, sea-level pressure  $P_0$  is reported only once every hour, necessitating an additional use of altimeter setting  $A$  available from most airport stations at special observation times. However, altimeter setting and sea-level pressure are basically different and their difference increases with station elevation when the air temperature is warmer or colder than the standard atmosphere.

Because 21 July was a hot summer day, altimeter settings were significantly higher than sea-level pressures at high elevation stations (see Fig. 20). At Laramie (LAR) for instance, the altimeter setting was 12mb higher than the sea-level pressure practically the whole day. If one tries to analyze pressure field by mixing  $P_0$  and  $A$ , the pressure pattern will turn into bubble highs and lows encircling reporting stations at high elevation.

In order to overcome this problem, the mean sea-level pressure  $\bar{P}_0$  at each station for the analysis period 07 - 18MST (14 - 01Z) was computed first and plotted on the map, along with the mean vector wind at the station. Then the isobars of  $\bar{P}_0$  were contoured for every millibar by using all available stations. Likewise, the mean altimeter setting  $\bar{A}$  was computed at each available station for the same period, finding, as expected, that  $\bar{A}$  is 2 to 12mb higher than  $\bar{P}_0$ .

Time sections in Fig. 21 were obtained by shifting the value of  $\bar{A}$  downward until it coincides with  $\bar{P}_0$ . Hourly- and special-observation pressures were connected with full lines when pressure traces were available. If not available, pressures were connected with dashed lines. The top diagram shows an incipient stage of the mesohigh which gave rise to the pressure

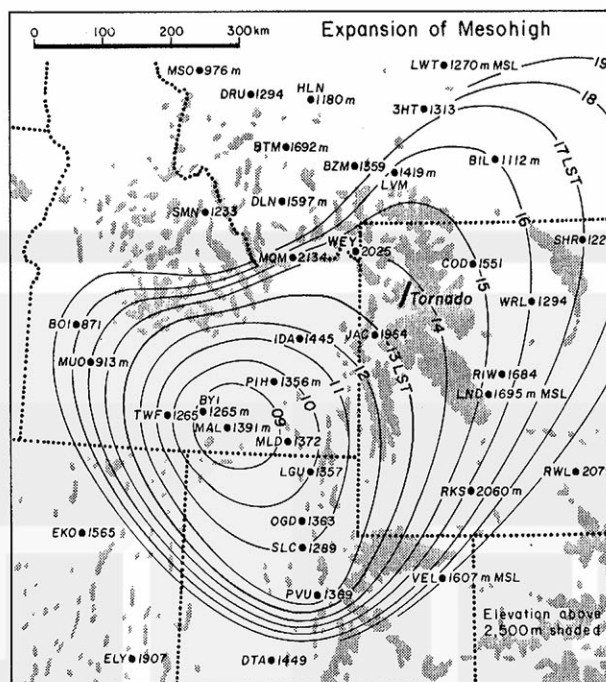


Fig. 19. Hourly isochrones of the mesohigh boundary on 21 July 1987. Areas of mountains above 2500m are shaded.

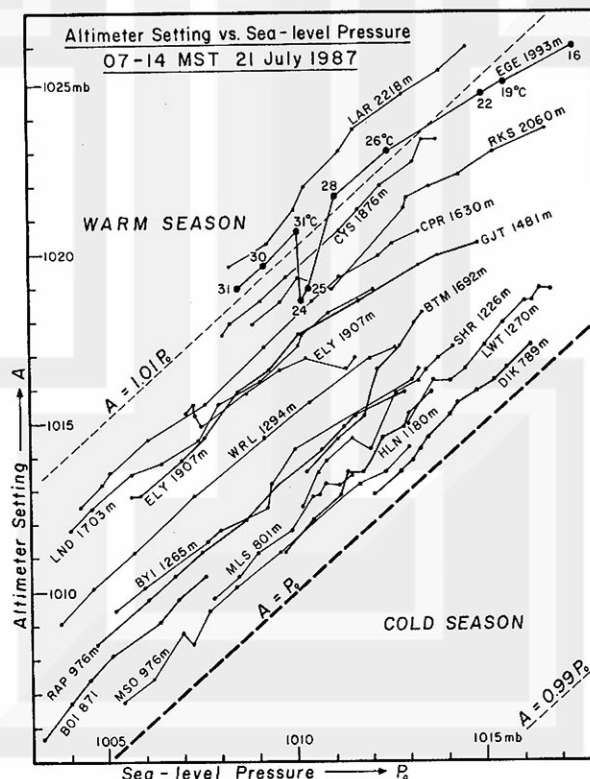


Fig. 20. Altimeter setting and sea-level pressure reported hourly from surface stations in the northwestern Rockies. Altimeter setting, computed from standard atmosphere, is higher than sea-level pressure in warm season because the latter decreases as temperature increases. At Eagle (EGE), Colorado,  $A - P_0$  decreased by 2mb corresponding to 4 - 7°C cooling. The decrease was attributed to the increase of  $P_0$ .

increase between 0900 and 1230MST and the corresponding outflow winds at Burley (BYI), Idaho. The same mesohigh affected Pocatello (PIH), Idaho 100km to the northeast of BYI, causing a strong outflow centered at 1315MST.

At Jackson Hole Airport, pressure kept falling since 0800MST, reaching a minimum at 1300MST when the mesocyclone center was passing nearest to the station. Cody (COD), Wyoming was located to the north of the cold front, the wind direction before the mesohigh was from the northerly direction, and pressure rose over 4mb during the passage of the mesohigh.

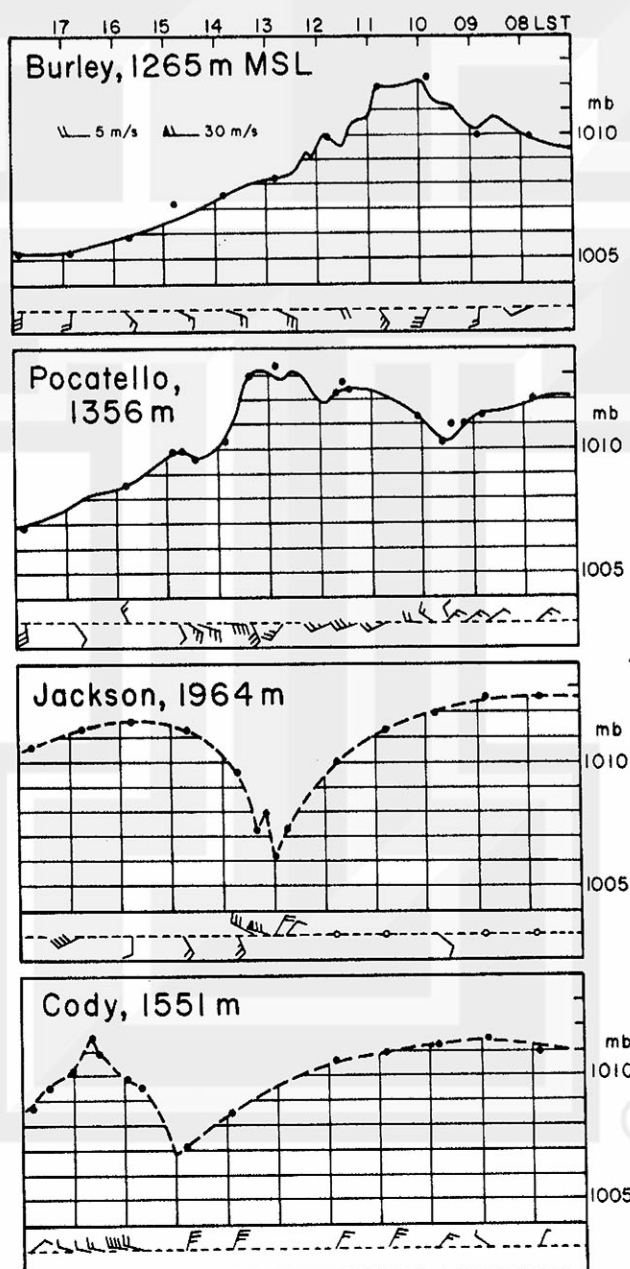


Fig. 21. Time sections at BYI, PIH, JAC, and COD, showing the expansion and advancement of the mesohigh. The parent mesocyclone of the tornado passed east-southeast of JAC at 1300MST.



#### d. Mesoanalysis of the mesocyclone

Although JAC was the only station within the mesocyclone circulation, the mesoscale pressure field can be delineated by the standard mesoanalysis technique of time-space conversion. First, the translational speed of the mesocyclone cloud was estimated to be 25 m/s, based on the winds aloft and the motion of the overshooting cloud top measured by GOES East and West. Second, the direction of the cloud motion was assumed from the 204° azimuth, the orientation of the tornado damage in Fig. 3.

Under the assumption that the mesocyclone moved at the constant rate of 25 m/s from 204°, positions of the cloud at 10 min interval are shown in the upper map of Fig. 22. The best estimate of the touchdown time was 1328MST (2028Z) and the liftoff time, 1354MST (2054Z). This map shows that the mesocyclone center passed 20 km east-southeast of JAC at 1300MST (2000Z) when JAC reported the minimum pressure. The lower map presents the mesocyclone, mesohigh, and cold front discussed earlier. In analyzing the pressure field, pressure-trace tendencies at reporting stations were used as additional information for determining pressure pattern from time sections.

It should be emphasized that the mesocyclone cloud was located near the intersection of a warm front and a mesohigh boundary. The importance of severe storm formation at the intersection of arc clouds or mesohigh boundaries has been emphasized by Purdom (1986), and the process of this mesocyclone formation appears to be very similar to his conceptual model.

#### 4. Infrared temperature of the parent cloud

The Teton-Yellowstone Tornado was spawned by a tornadic mesocyclone. This mesocyclone cloud, a rotating thunderstorm, is called in this paper the parent cloud of the tornado, or the parent cloud. Infrared and visible pictures in Fig. 23 do not show the parent cloud hidden inside a vast area of high-level cirrus cloud extending from Idaho, Wyoming, and Montana. These pictures, started at 1400MST, scanned the tornado area several minutes later at 1404MST (2104Z), and the tornado ended 10 min before the scan time.

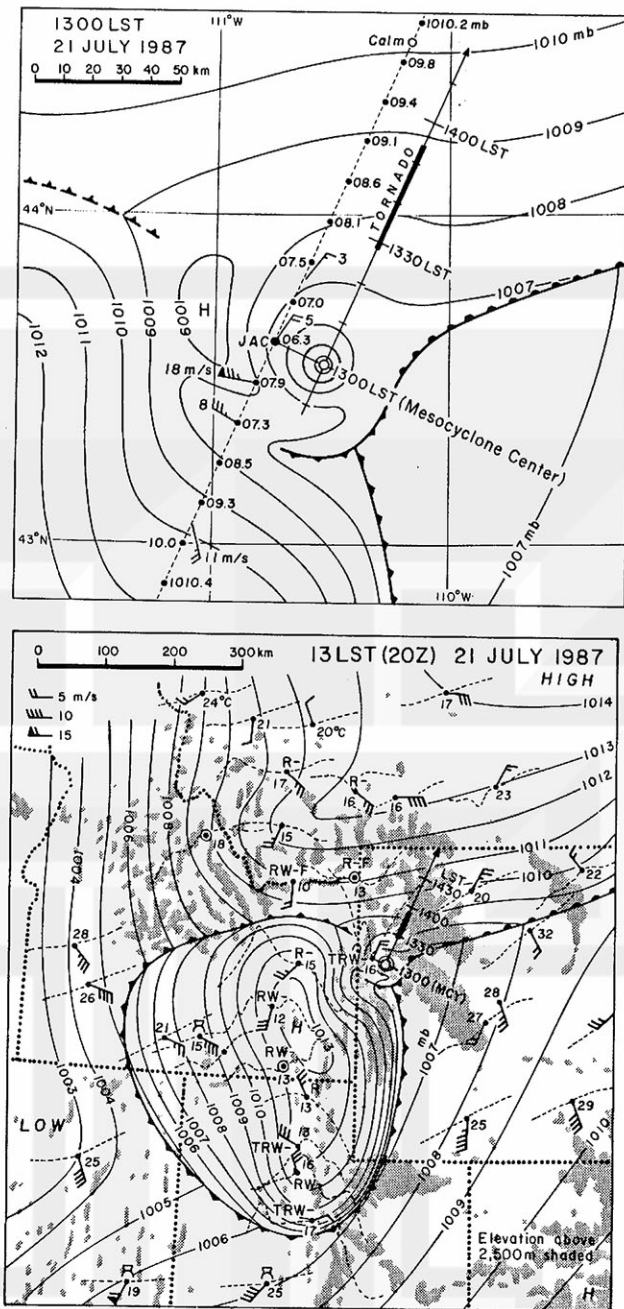


Fig. 22. Upper map: Isobars and path of the mesocyclone determined by combining the damage path and surface weather observations at JAC. Lower map: Mesoanalysis map at 1300MST showing the location of the mesocyclone (MCY) in relation to cold front and mesohigh boundary. Dashed lines at surface stations are pressure tendency traces.

#### a. Gridding at the cloud top level

Operational GOES pictures include the grids which coincide with geographic features at sea level. As a result, objects at high elevations deviate toward the direction away from the subsatellite point on the equator. The amount of deviation increases in proportion to the MSL height.

The visible picture depicts mountain waves behind high mountain ranges oriented perpendicular to the strong moisture flow from Utah and Colorado to Wyoming. These ranges are Unita Mountains (4124m), Wind River Range (4208m) west of LND, and Big Horn Mountains (4104m). Numerous cloud streets over the high Rockies were disappearing along the foothills. The northward flow toward the parent cloud converged orographically while passing over Green River Valley between Wind River Range and Salt River Range, north-south mountains on the Wyoming side of the Idaho border (see Fig. 22).

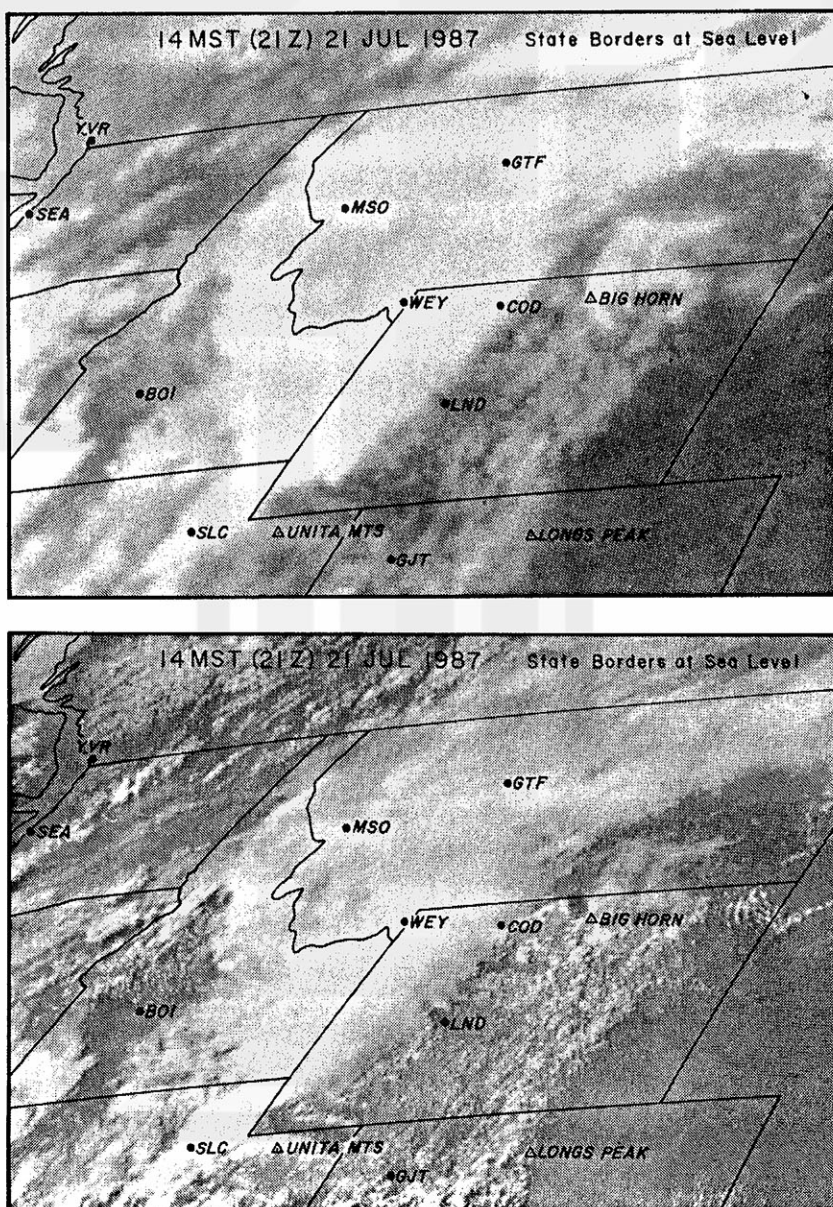


Fig. 23. Infrared (upper) and visible (lower) pictures at 1404MST scan time, 10 min after the end of the tornado which was on the ground between 1328 and 1354MST. State borders drawn are at sea-level.



Let  $\zeta$  be the geocentric angle between subsatellite point and cloud. It can be computed by a spherical trigonometric equation,

$$\cos \delta = \cos \phi \cos(\theta - \theta_0). \quad (1)$$

where  $\phi$  and  $\theta$  are latitude and longitude of the cloud, respectively, and  $\theta_0$ , the subsatellite longitude. By using the data for the parent cloud at 1400MST,  $\phi = 44.3^\circ\text{N}$ ,  $\theta = 110.1^\circ\text{W}$ , and  $\theta_0 = 74.7^\circ\text{W}$ , we have

$$\delta = \cos^{-1} 0.583 = 54.3^\circ. \quad (2)$$

The zenith angle,  $\zeta$ , of GOES East at the parent cloud is computed by solving an oblique plane triangle, including satellite, parent cloud, and earth's center. Thus we have

$$\zeta = 63.5^\circ. \quad (3)$$

The satellite-viewed position of the cloud top will deviate from sea-level grid by

$$P = h \tan \zeta \quad (4)$$

where  $P$  denotes the length of the deviation vector. For computation equations on the ellipsoidal earth, refer to Fujita (1982). Using the 14km height of the parent cloud and the zenith angle in Eq. (3), we obtain

$$P = 14 \times 2.01 = 28\text{km}. \quad (5)$$

This means that sea-level grids cannot be used in locating the parent cloud, because the error is 28km (17.5mi).

#### b. Infrared isotherms on elevated grids

In determining the accurate position of the parent cloud in cloud-top temperature field, the state boundaries in Fig. 24 were gridded at 14km MSL, the estimated height of the highest cloud identified by a small triangle encircled by a  $-63^\circ\text{C}$  isotherm.

A new technique of 3-D isotherms was developed by using black and white isotherms on gray background. In selecting the colors of isotherms, it was assumed that the illumination light shines from the northwest on the topographic height proportional to the negative value of IR temperatures in  $^\circ\text{C}$ . This means that the coldest temperature is identified as the highest point of the 3-D topography.

In emphasizing small temperature variations inside anvil clouds, isotherms were drawn at a  $10^\circ\text{C}$  interval between  $+30^\circ\text{C}$  and  $-50^\circ\text{C}$ ,  $2^\circ\text{C}$  interval between  $-50^\circ\text{C}$  and  $-60^\circ\text{C}$ , and  $1^\circ\text{C}$  interval below  $-60^\circ\text{C}$ .

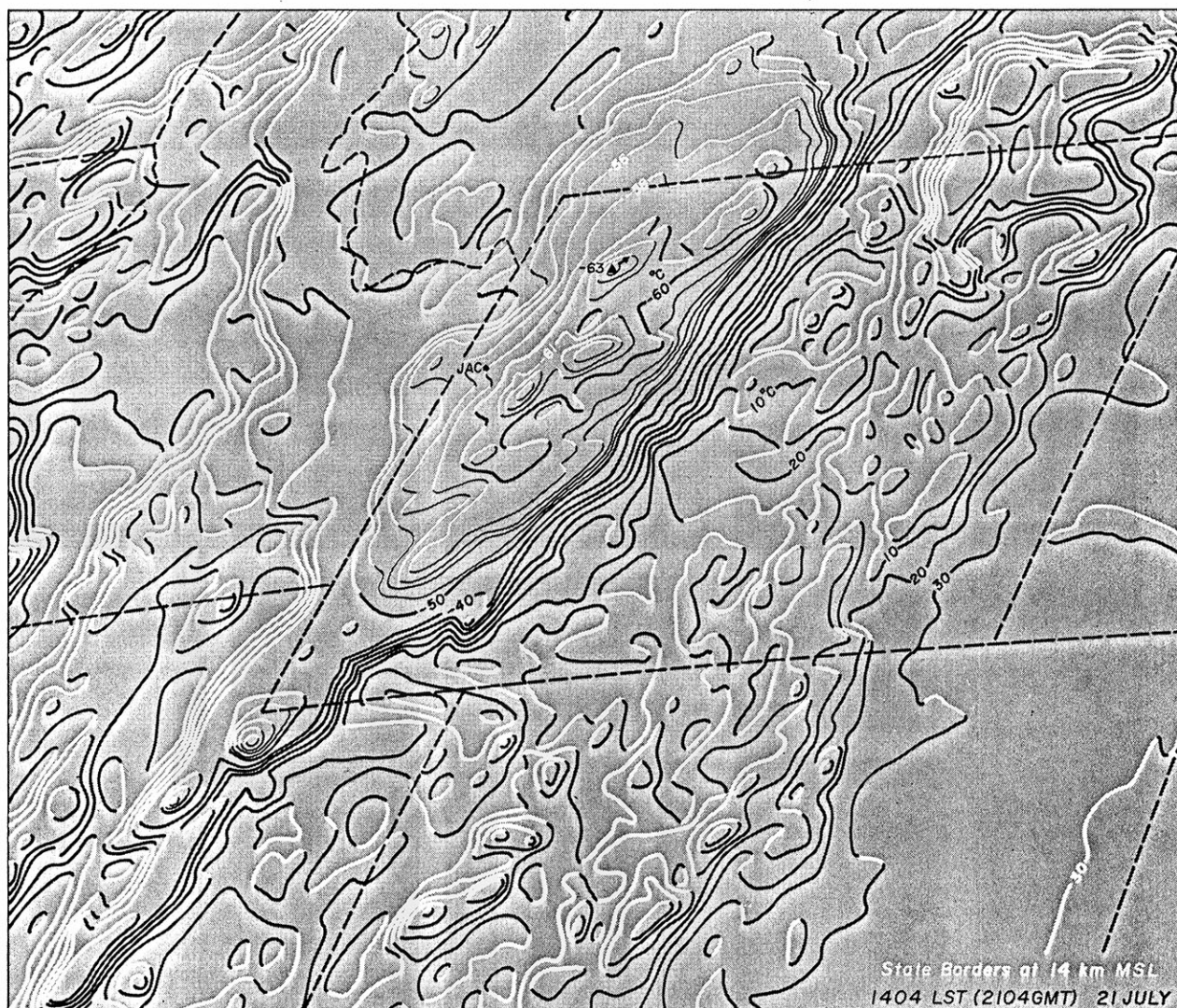


Fig. 24. A 3-D pattern of infrared temperature at 1404MST scan time. State boundaries in this figure are gridded at 14km MSL.

### c. Parent cloud of the Teton-Yellowstone Tornado

An attempt was made to single out the temperature pattern of the overshooting top of the parent cloud which left behind a 39km long damage path. Five pictures from GOES East and West were analyzed with  $1^{\circ}\text{C}$  contours. As shown in Figs. 25 and 26, a small but distinct cloud top moved directly over the damage area at 25 m/s. Assuming that the damage occurred beneath this cloud, the touchdown and liftoff times of the tornado were computed as 1328MST and 1354MST, respectively.

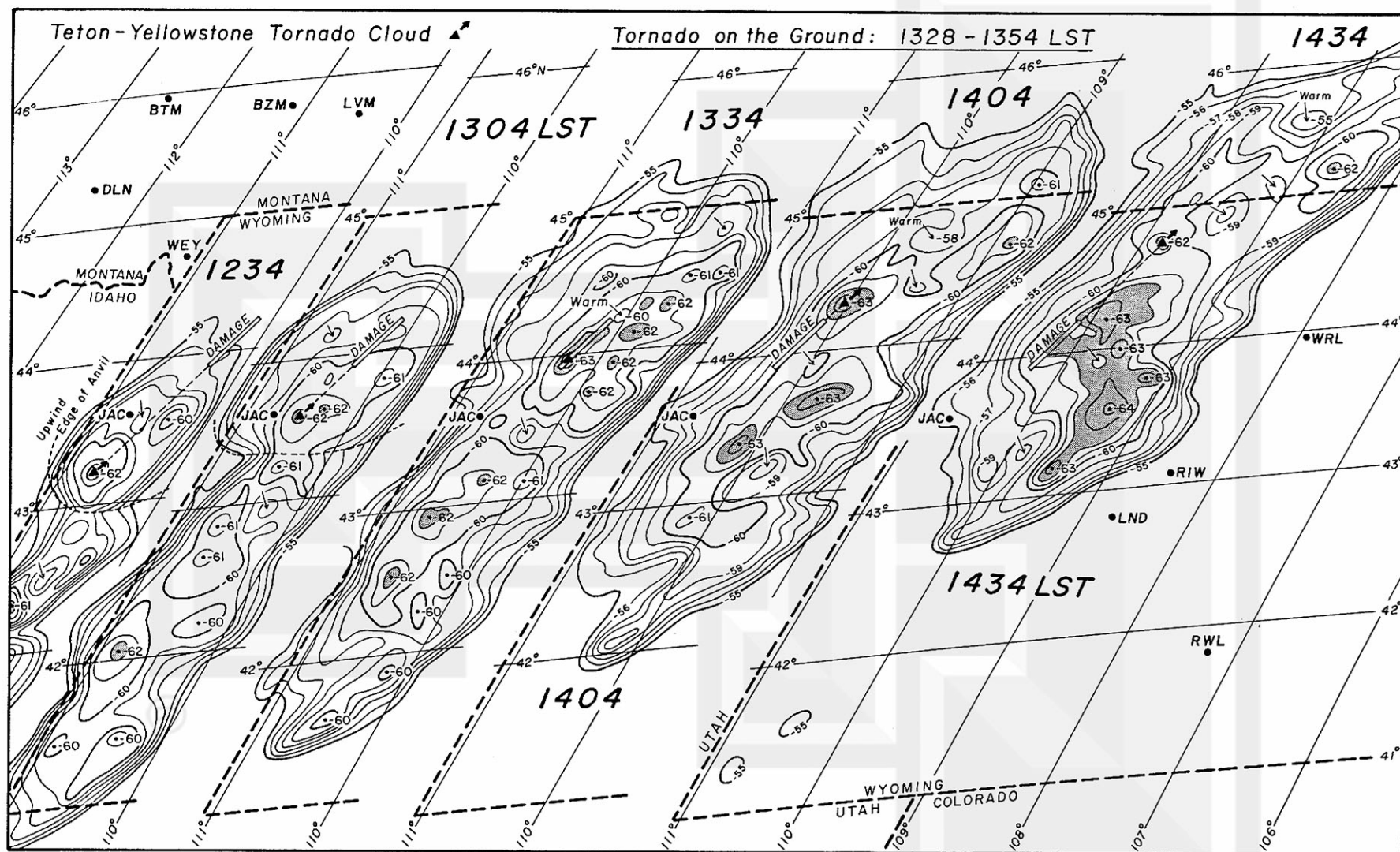


Fig. 25. Isotherms of the anvil-cloud complex derived from GOES East infrared temperature. Times indicated are scan time in MST. Geographic grid lines are computed at 14km MSL on the ellipsoidal earth.



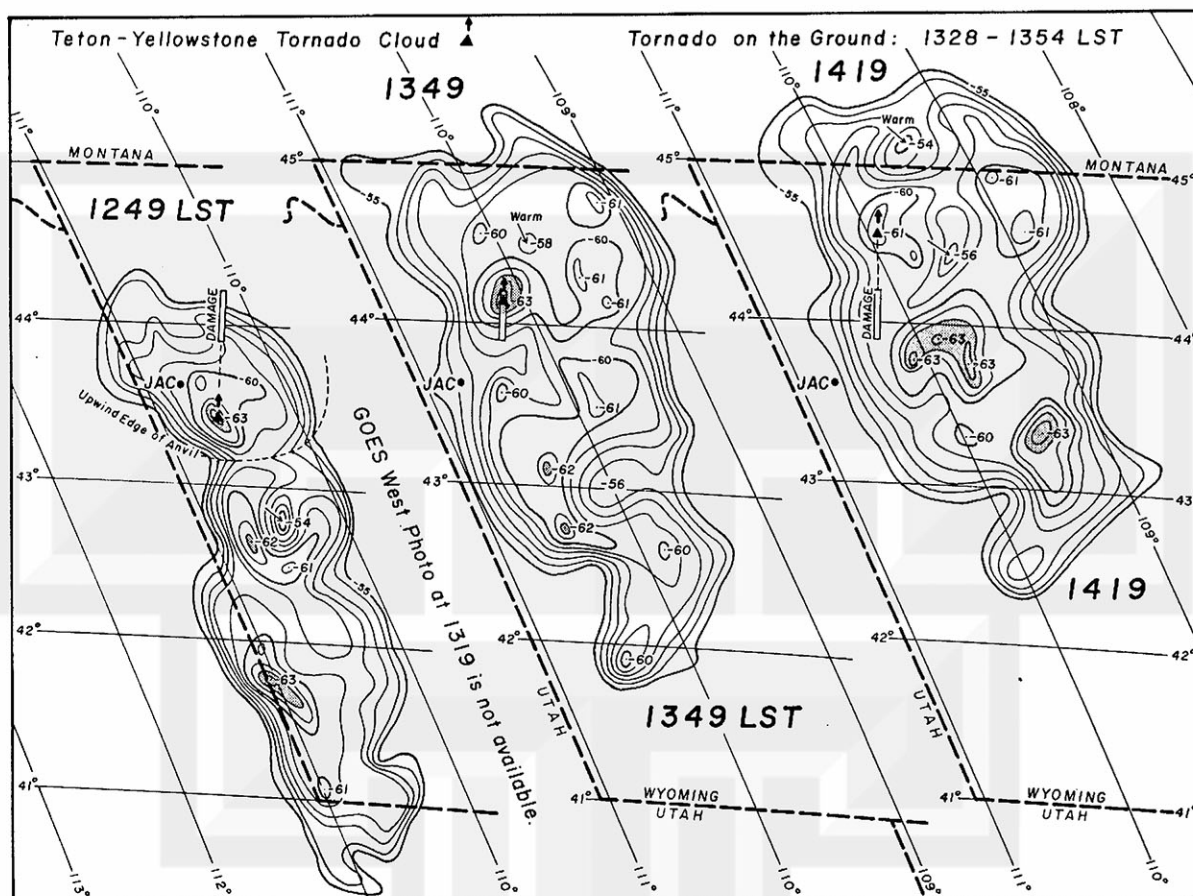


Fig. 26. Isotherms of the anvil-cloud complex derived from GOES West infrared temperature. Times indicated are scan time in MST. Geographic grid lines are computed at 14km MSL on the ellipsoidal earth.

The first picture (IR temperature pattern) by GOES East at 1234MST shows a growing anvil cloud with its upwind edge in the vicinity of 43°N latitude and 111°W longitude. A -62°C cloud top on the upwind side of the anvil was moving toward the damage area. At 1249MST, 15 min after the first picture, GOES West depicted a -63°C cloud top and the upwind edge of the anvil cloud from a different perspective, looking from above the Pacific.

A -62°C cloud top was to the east of JAC at 1304MST, 4 min after JAC reported the lowest sea-level pressure, 1006.1mb. At 1310MST, the station observed a 26 m/s (58mph) gust from the west. The parent cloud was directly over the worst damage between Gravel Ridge and Enos Lake at this time. The -63°C cloud in the GOES West picture at 1349MST was near the end of the damage area and the tornado lifted off 5 min after this picture.

At 1404MST, 10 min after the end of the tornado, the cloud-top temperature was still cold,  $-63^{\circ}\text{C}$ . As far as we know, no damage was found beneath this cold cloud. The GOES West picture at 1419MST shows a  $-61^{\circ}\text{C}$  top and GOES East picture at 1434MST, a  $-62^{\circ}\text{C}$  top, indicating weakening of the parent cloud.

Table 4 summarizes the pixel counts of the parent cloud in eight GOES East and West pictures from digital data analyses. This result shows clearly that the  $-61^{\circ}\text{C}$  or colder pixels increased about 10 min before the tornado and decreased rapidly 10 min after the tornado, reaching a peak during the tornado. Although pixel counts are low, similar changes in pixel characteristics occurred at  $-62^{\circ}\text{C}$  and  $-63^{\circ}\text{C}$  temperatures.

Table 4. Pixels of cloud-top temperatures above the Teton-Yellowstone Tornado cloud. Numbers in the table denote the cumulative counts of pixels with temperatures of  $-61$ ,  $-62$ ,  $-63$ , and  $-64^{\circ}\text{C}$  or lower. MST denotes the scan time.

| MST  | GMT  | GOES | $-61^{\circ}\text{C}$ | $-62^{\circ}\text{C}$ | $-63^{\circ}\text{C}$ | $-64^{\circ}\text{C}$ | Remarks |
|------|------|------|-----------------------|-----------------------|-----------------------|-----------------------|---------|
| 1234 | 1934 | East | 5                     | 3                     | -                     | -                     |         |
| 1249 | 1949 | West | 8                     | 4                     | 2                     | -                     |         |
| 1304 | 2004 | East | 15                    | 2                     | -                     | -                     |         |
| 1334 | 2034 | East | 24                    | 8                     | 2                     | -                     | Tornado |
| 1349 | 2049 | West | 19                    | 12                    | 2                     | -                     | Tornado |
| 1404 | 2104 | East | 27                    | 11                    | 1                     | -                     |         |
| 1419 | 2119 | West | 4                     | -                     | -                     | -                     |         |
| 1434 | 2134 | East | 6                     | 2                     | -                     | -                     |         |

#### d. Formation and motion of the warm wake

Another interesting evidence in the parent cloud is the formation and motion of a warm wake. The warm wake was first detected at 1334MST in GOES East picture, 30km downwind from the  $-60^{\circ}\text{C}$  parent cloud. As shown in Fig. 27, the temperature of the wake increased from  $-60^{\circ}\text{C}$  to  $-55^{\circ}\text{C}$  when the wake was moving away from the parent cloud, being accelerated from 35 m/s to the maximum 48 m/s. As a result, the distance between the cold top and the wake increased to 105km at 1434MST. Both top and wake moved from the  $204^{\circ}$  azimuth, the direction of the tornado.

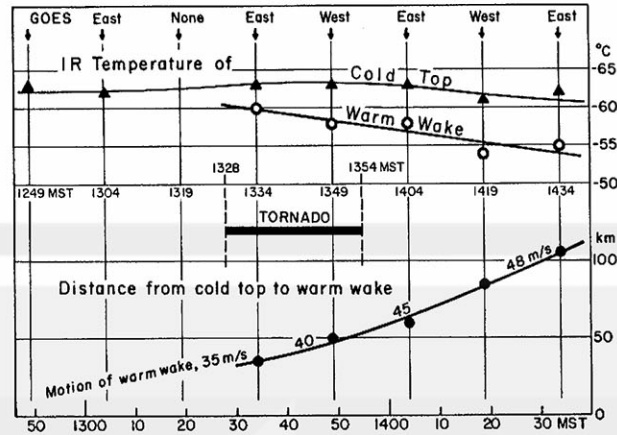


Fig. 27. Infrared temperature of the parent cloud-top and its warm wake. The cold top moved at 25 m/s while the motion of the warm wake accelerated from 35 m/s to 48 m/s.

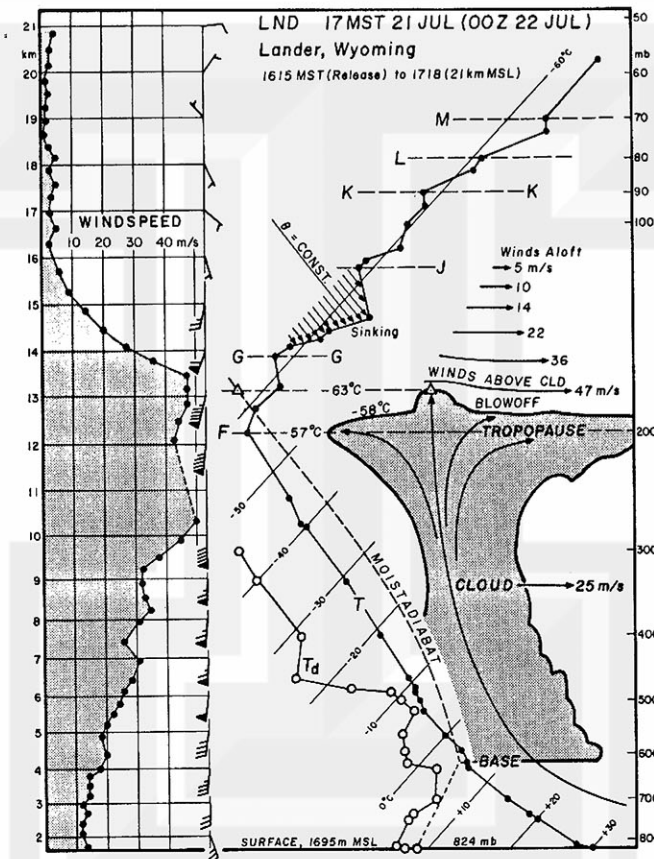


Fig. 28. A schematic cross section of the parent cloud. The lowest pixel temperature,  $-63^{\circ}\text{C}$ , corresponds to the moist-adiabatic temperature at 13.1 km MSL. Because the IFOV is much larger than the small overshooting top, the highest top of the parent cloud was assumed at 14 km MSL. Note that the 47 m/s wind above the anvil extended 13.5 km MSL, suggesting that the wind could transport the stratospheric cirrus atop the anvil cloud.



A schematic vertical cross section of the parent cloud in Fig. 28 was constructed to determine the characteristics of the parent cloud in relation to the environmental winds and temperature from the LND sounding at 1615-1718MST (0000Z sounding). The 25 m/s cloud motion corresponds to the winds aloft at 6.0km MSL (4.3km AGL) and the final drifting speed of the warm wake is very close to the 47 m/s wind atop the anvil cloud.

The characteristic motion of the warm wake suggests that the wake could consist of the stratospheric cirrus photographed and reported by Fujita (1982). His observations from the research Lear Jet confirmed that the jumping cirrus shoots up, like a geyser, into the stratosphere from the anvil surface when the overshooting domes atop severe thunderstorms collapse violently. It may be postulated that jumping cirrus warms up inside the lowermost stratosphere while reaching 2 to 3 km above the anvil top. However, quantitative values of the density, temperature, and emissivity which give rise to the IR temperature of the warm wake have not yet been known.

Due to low stratospheric winds, especially in warm seasons, the jumping cirrus accumulates above the anvil cloud, increasing the infrared temperature behind the top. As time goes by, the accumulated jumping cirrus drifts downwind with the anvil-top wind. In this case, the windspeed over LND was 47 m/s, but it could be very weak in other cases, resulting in a significant accumulation of the stratospheric cirrus in late spring and summer when the anvil-top winds are either weak or calm.

## 5. Upper-air cross sections

The Teton-Yellowstone Tornado occurred beneath the jet stream around a 200mb cyclone centered over the Oregon coast. The jet extended from over San Francisco, California to southern Canada, passing over SLC and GTF where the maximum wind speed at 11.8km MSL (212mb) was 57 m/s.

### a. Anvil-top winds at 200mb and 100mb

The 100 and 200mb winds at 17MST (00Z) superimposed upon the visible picture at 1630MST show strong jet stream winds at 200mb. At 100mb however, the wind speed dropped to less than 4 m/s directly over the area of the high winds at 200mb (see Fig. 29).

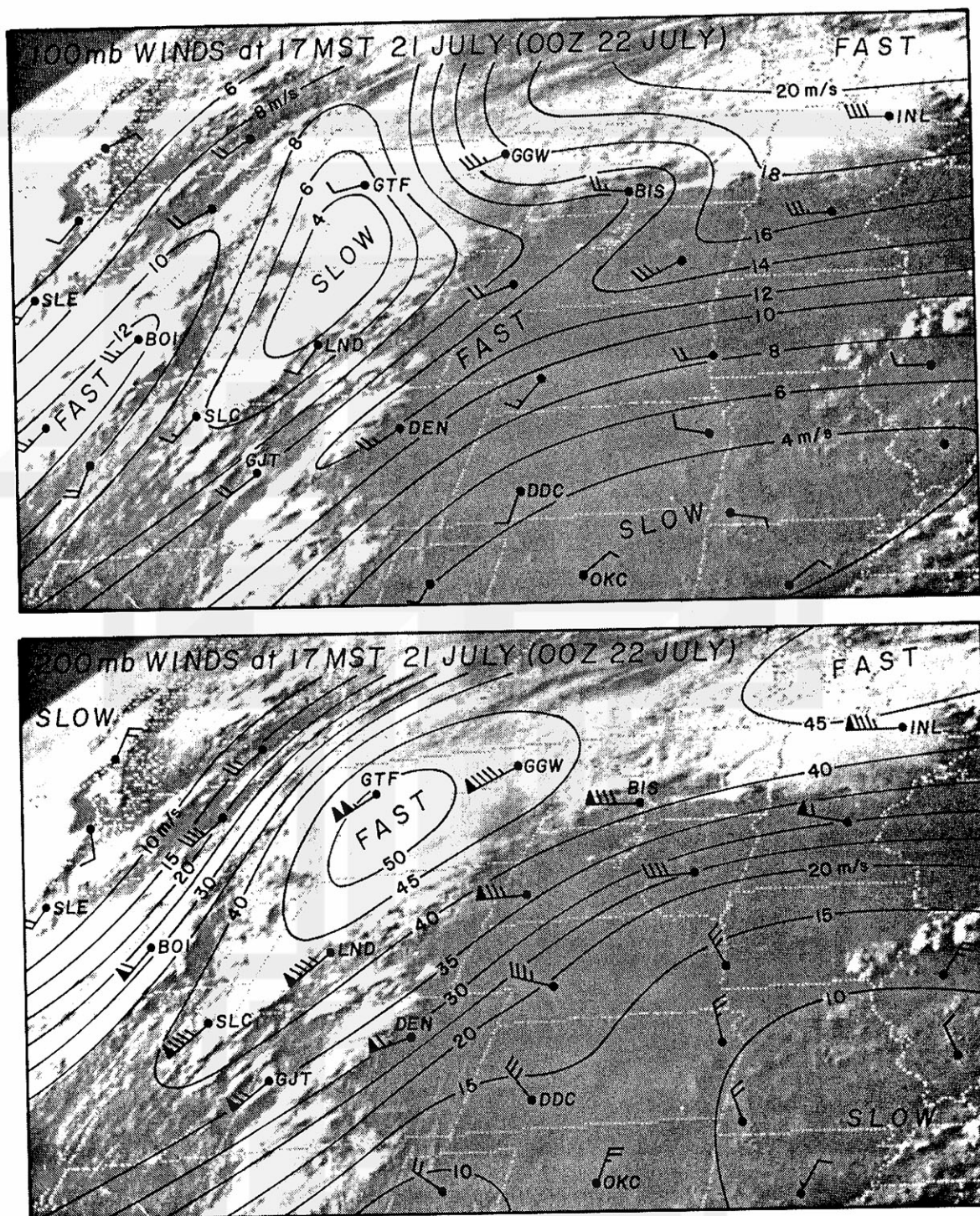


Fig. 29. Jet stream winds at 200mb and slow winds at 100mb at 17MST (00Z) superimposed upon the GOES East pictures started at 1630MST (2330Z). A slow-wind area at 100mb (upper picture) is located directly above the high-wind core.

This phenomenon is seen more effectively in an upper-air cross section along the line, SLM-BOI-SLC-LND-GJT-DDC-OKC (see Fig. 18). The vertical cross section in Fig. 30 shows a 45 m/s core of the jet stream located at 12.5km MSL. This core is topped by a core of slow winds, less than 5 m/s at 16.5km MSL. Are these high-wind and low-wind cores dynamically related?

#### b. Vertical cross sections

Before attempting to answer this question, we shall examine the stratospheric wind above 100mb. Isotachs in Fig. 30 show the existence of the level of minimum wind speed (LMIWS) at 110mb over OKC, 70mb over DEN,

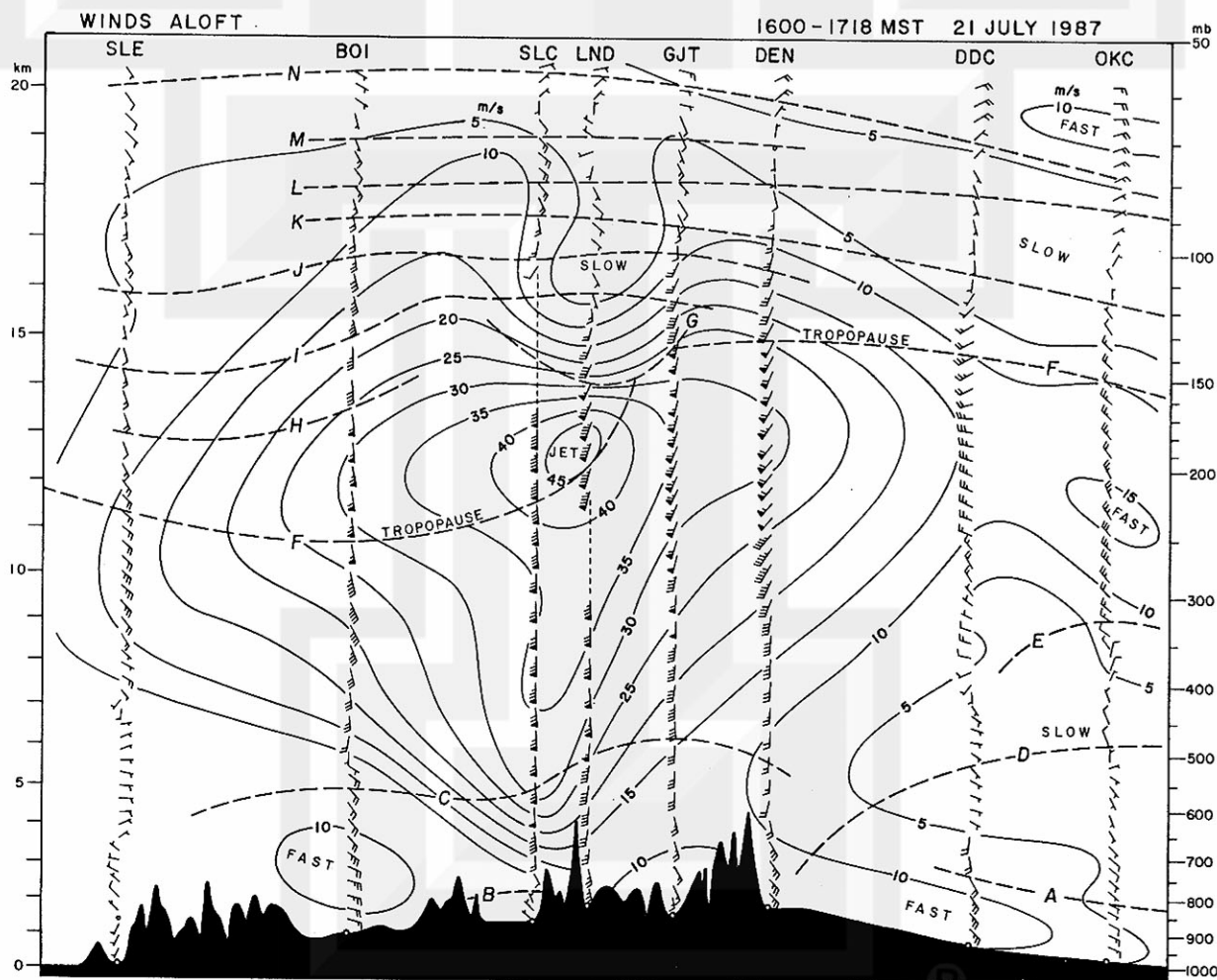


Fig. 30. A vertical cross section of winds aloft at 1700MST on 21 July 1987 (00Z 22 July 1987). The high-wind core above LND is topped by a low-wind core. The concave-upward line G denotes the boundary between high- and low-wind cores.





A vertical cross section of potential temperature in Fig. 32 will provide another way of identifying a large-scale sinking on the left side and a mesoscale sinking above the storm cloud. A combined examination of Figs. 30, 31, and 32 gives a definite impression that the suspected mesoscale sinking could cause both slow-wind core and warming depicted by these vertical cross sections.

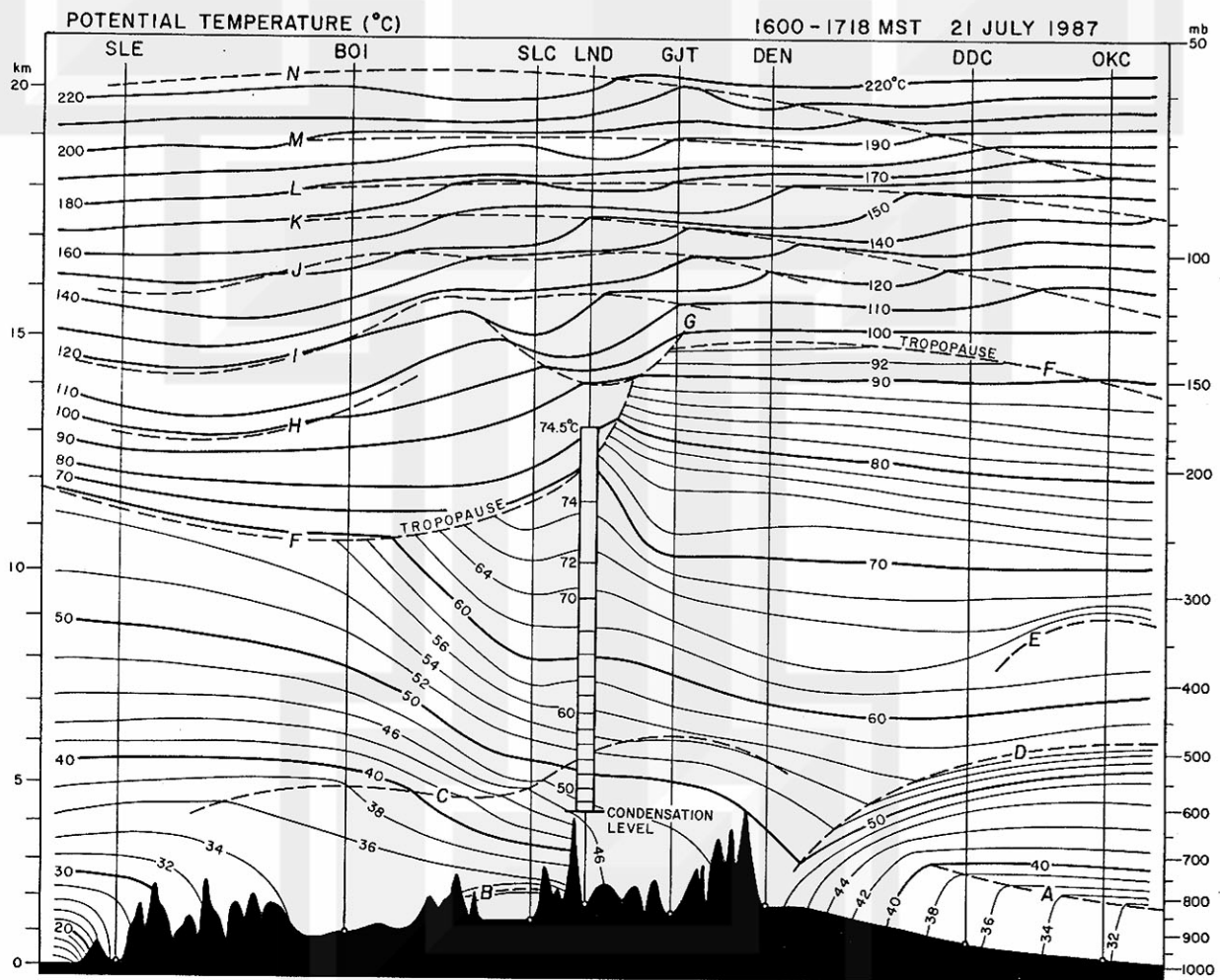


Fig. 32. A vertical cross section of potential temperature (°C). Dashed lines F through N denote the lines of minimum temperature located at the bases of inversions identified on adiabatic charts.

Based on this evidence, along with that reported earlier by Fujita (1982), we may postulate an atmospheric process in which a slow sinking motion above a severe-storm anvil could induce a warm wake above the anvil top. When the jumping cirrus from overshooting areas moves into the region of the slow wind and warm temperature, a massive stratospheric cirrus will accumulate above the anvil cloud, downwind of the overshooting domes. When this stratospheric cirrus, warmer than the anvil-top temperature, forms and drifts above the cold anvil top, it will be observed as a drifting warm wake.

Although this case study is not sufficient in proving the hypothesis on the formation mechanism of the mesoscale core of low wind and warm temperature, as well as the warm wake, similar analyses of other storms over western mountains could lead to a better understanding of this interesting phenomenon in the lowest stratosphere above the Teton-Yellowstone tornado cloud.

## 6. Summary and conclusions

Prior to the occurrence of this remote-area tornado, Mr. Fred Ostby of the National Severe Storms Forecast Center (NSSFC) and the author noticed that the overall intensity of U.S. tornadoes has been declining steadily during the past several years. Meanwhile, a number of destructive tornadoes has been reported from unexpected locations. This research revealed that the number of F3-F5 tornadoes decreased dramatically from 65 to only 15 in six years, 1982-87 (see Table 1).

The purpose of this paper is to document the rare event of the Teton-Yellowstone Tornado, the strongest and the longest storm which crossed the Continental Divide above 3000m MSL. In documenting the damage in the remote wilderness, the entire damage area was flown by a photographic aircraft for taking stereo-pair pictures in recording literally every single tree in the forest. Directions of damaging winds, as identified by fallen trees, were mapped in detail, identifying at least 4 tornadic swirls and 72 microburst outflows inside the 39.2km-long and 2.5km-wide swath.



It was found that the parent cloud with  $-63^{\circ}\text{C}$  cloud-top temperature moved over the damage area at 25 m/s, causing the damage in 26 min between 1328 and 1354MST (2:28 to 2:54 p.m. MDT). The parent cloud formed at the intersection of the mesohigh boundary and a warm front. In spite of difficulties in performing the isobaric analysis in mountain areas, altimeter settings were used in completing a series of mesoanalysis maps of the mesohigh. Meanwhile, a method of 3-D analysis of the cloud-top temperature was developed and utilized in tracking cold cloud tops in GOES East and West pictures.

It was concluded that an insight analysis of the tornado damage, the parent cloud, and its environment is useful in learning the nature of different types of tornadoes in the Rockies. This research will also provide both storm forecasters and Forest Service officials with the extent of an unexpected but a possible damage which could occur during one's lifetime.

#### Acknowledgements

The author is grateful to the U.S. Forest Service of Teton Wilderness for providing important storm information and in assisting the site visits by Messrs. Brian E. Smith, James W. Partacz, and Bradley S. Churchill, staff members of the Wind Research Laboratory, The University of Chicago. After his low-altitude aerial photography, Mr. Brian Smith performed a painstaking identification of his pictures in completing the four local damage maps. As part of satellite data analysis, Mr. Jaime J. Tecson generated grid-print maps of GOES East and West cloud-top temperature.

This research has been sponsored by the National Science Foundation under Grant ATM85-16705, the National Oceanic and Atmospheric Administration/NESDIS under Grant NA85-AADRA064, and the National Aeronautics and Space Administration under Grant NGR 14-001-008.

## REFERENCES

- Brown, R.A., W.C. Bumgarner, K.C. Crawford and D. Sirmans, 1971: Preliminary Doppler velocity measurements in a developing radar hook echo. Bull. Amer. Meteor. Soc., 52, 1186-1188.
- Burgess, D.W., L.D. Hennington, R.J. Doviak and P.S. Ray, 1976: Multi-moment Doppler display for severe storm identification. J. Appl. Meteor., 15, 1302-1306.
- Flora, S.D., 1954: Tornadoes of the United States. University of Oklahoma Press, Norman, Oklahoma, 221 pp.
- Fujita, T.T., 1981: Tornadoes and downbursts in the context of generalized planetary scales. J. Atmos. Sci., 38, 1511-1534.
- \_\_\_\_\_, 1982: Principle of stereoscopic height computations and their applications to stratospheric cirrus over severe thunderstorms. J. Meteor. Soc. Japan, 60, 355-368.
- \_\_\_\_\_, 1987: U.S. Tornadoes: Part I, 70-year statistics. SMRP Paper No. 218, The University of Chicago, 122 pp. [NTIS PB87-127742, Library of Congress Catalogue Card No. 86-51637].
- Garrett, R.A., and V.D. Rockney, 1962: Tornadoes in northern Kansas, May 19, 1960. Mon. Wea. Rev., 90, 231-240.
- Purdom, J.F.W., 1986: Satellite contributions to convective scale weather analysis and forecasting. 11th Conf. Weather Forecasting and Analysis, Kansas City, Mo., 295-314.
- Tornado Maps, 1986-87: Storm Data. NOAA/NCDC Publ., 24 monthly issues.